

Linear and Nonlinear Dynamics of Self-Consistent Collisionless Tearing Modes in Toroidal Gyrokinetic Simulations

F. Widmer,^{1, a)} E. Poli,^{2, 3} A. Mishchenko,⁴ A. Ishizawa,³ A. Bottino,² and T. Hayward-Schneider²

¹⁾Headquarters for Co-Creation Strategy, National Institutes of Natural Sciences, Minato-ku, Tokyo 105-0001, Japan^{b)}

²⁾Max Planck Institute for Plasma Physics, 85748 Garching, Germany

³⁾Graduate School of Energy Science, Kyoto University, Uji, Kyoto 611-0011, Japan

⁴⁾Max Planck Institute for Plasma Physics, 17491 Greifswald, Germany

(Dated: October 21, 2024)

We investigate tearing modes (TM) driven by current density gradient in collisionless tokamak plasmas by using the electromagnetic gyrokinetic simulation code ORB5. We elucidate the TM width by simulations for flat profiles, as the absence of background diamagnetic flows implies a small rotation-speed, while finite-gradients are included to investigate the TM rotation. For flat profiles, the initial saturation width of nonlinearly driven magnetic islands is related to the TM linear growth rate; however, large islands in the initial saturation phase are prone to current density redistribution that reduces the island width in the following evolution. Island-induced $\mathbf{E} \times \mathbf{B}$ and diamagnetic sheared flows develop at the separatrix, able to destabilize the Kelvin-Helmholtz instability (KHI). The KHI turbulence enhances a strong quadrupole vortex flow that reinforces the island decay, resulting in a strong reduction of the island width in an eventual steady state. This process is enhanced by trapped electrons. For finite gradients profile, the TM usually rotates in the electron diamagnetic direction, but can change direction when the ion temperature gradient dominates the other gradients. The reduced growth of the TM by diamagnetic effects results in a moderate island size, which remains almost unchanged after the initial saturation. At steady state, strong zonal flows are nonlinearly excited and dominate the island rotation, as expected from previous theoretical and numerical studies. When β is increased, the TM mode is suppressed and a mode with the same helicity but with twisting parity, coupled with the neighboring poloidal harmonics, is destabilized, similar to the kinetic ballooning mode.

I. INTRODUCTION

Magnetic reconnection is an ubiquitous phenomenon in magnetized plasmas, from astrophysics to fusion plasma experiments. It changes the magnetic field topology leading to the appearance of magnetic island shaped structures.¹ The magnetic energy is released in the process and a lower energy plasma state is attained by the system.^{2,3} In fusion experiments, the nested magnetic flux surfaces configuration is violated by the appearance of magnetic islands. As the island grows radially in size, it provides radial shortcuts for the particle motion. The result is a flattening of the radial pressure profile, lowering the energy confinement.⁴⁻⁶

Magnetic islands can develop in tokamaks in the nonlinear phase of a current-driven tearing mode (TM), characterized by a positive tearing parameter $\Delta' > 0$.¹ Neoclassical Tearing modes (NTM) are of particular concern for present and future fusion devices as they can develop also for TM-stable current profiles ($\Delta' < 0$) as a consequence of the bootstrap-current perturbation arising from the pressure flattening mentioned above.⁷ NTMs often need an initial seed island, which is influenced by the island rotation through the polarization current, to grow,⁸⁻¹⁰ the classical tearing mode has the ability to further develop into an NTM by playing the role of the seed.¹¹ The dynamics of non-linear islands are known to be considerably altered by kinetic and toroidicity

effects even within a drift-kinetic or neoclassical picture.¹² This has prompted several studies in this sense, starting with the analysis of the plasma response to a prescribed magnetic island.¹³⁻²³

Meanwhile, a few self-consistent gyrokinetic investigations of the tearing instability and nonlinear evolution are available as well.²⁴⁻²⁷ We mention for completeness that several gyrokinetic studies of the tearing instability in slab geometry have been performed as well.²⁸⁻³² As it can be surmised, the self-consistent evolution of the toroidal tearing mode in a turbulent environment exhibits an extremely rich dynamics.⁵ At the same time, the computational effort required by gyrokinetic simulations in this context is huge, since the electron dynamics needs to be resolved, as well as the different time scales associated with turbulence and tearing mode evolution. Moreover, for collisionless tearing modes, the violation of the frozen-in condition needed for reconnection is due to the finite electron inertia, and the collisionless skin depth of the electron must be resolved. Thus, although such global multi-scale simulations resolving simultaneously drift and MHD-like instabilities are becoming more and more feasible, see e.g.³³ and references therein, extended parameter scans are still very demanding.

In this paper, we investigate the dynamics of current-driven tearing modes in toroidal geometry employing gyrokinetic simulations with the gyrokinetic particles-in-cell (PIC) code ORB5.^{34,35} In order to counteract the computational problems mentioned above, we follow a twofold approach. On one hand, we relax the physical constraint on the mass ratio, increasing the electron mass by one order of magnitude in many of the simulations presented here. On the other hand, we limit the simulations to vanishing to

^{a)}Guest researcher at Max Planck Institute for Plasma Physics, 85748 Garching, Germany

^{b)}Electronic mails: f.widmer@nins.jp and fabien.widmer@ipp.mpg.de

mild density and temperature gradients, below the threshold for linear micro-turbulence instability. For both linear and nonlinear dynamics of the collisionless tearing mode in a circular, large aspect ratio tokamak, we investigate the linear collisionless tearing mode growth rate, island saturation mechanisms and rotation frequency through extensive parameter scans (density and temperature gradients, mass ratio, plasma β_e , etc.). This study is not just propaedeutic to the investigation of the interaction between turbulence and tearing modes discussed above. We will show that, despite these simplifying assumptions, new properties of the instability are revealed; in particular the interaction with other modes can appear both linearly at high enough β_e and nonlinearly due to the generation of turbulence around the island separatrix for strongly-driven modes. This turbulence exhibits features typical of the Kelvin-Helmholtz instability (KHI) and its evolution changes significantly depending on the presence or absence of electron trapping in the tokamak magnetic field.

Another topic addressed in this paper is the island rotation, which impacts the contribution both of the polarization current,³⁶ which is believed to play an important role for the NTM modeling, evolution and threshold,^{5,37–41} and of the bootstrap current (at least in small islands).^{12,42,43} Determining the TM mode drive and rotation frequency is thus necessary to properly model NTMs. In the presence of background gradients, diamagnetic effects determine the rotation of the TM in the linear phase,^{44,45} referred then as a drift-tearing mode, and can also reduce drastically the growth rate. In the nonlinear phase, the determination of the rotation is more subtle.^{46,47} For instance, a set of reduced two-fluid equations describing drift-tearing mode demonstrated that the tearing mode frequency was proportional to the diamagnetic drifts, the $\mathbf{E} \times \mathbf{B}$ flow, the background magnetic field geometry and the plasma resistivity.⁴⁸ Numerical simulations of two dimensional reduced MHD confirmed that the frequency is dictated by the diamagnetic drifts during the linear growth,⁴⁹ while being controlled by the $\mathbf{E} \times \mathbf{B}$ contribution at saturation. Additionally, the plasma β (ratio of kinetic to magnetic pressure) was shown to contribute to the island rotation through an amplification of the Maxwell stress.⁴⁹ The rotation frequency of the tearing (linear phase) and the island (saturation) were confirmed by two dimensional simulations of four fields models equations in slab geometry, including parallel ion motions as well as ion and electron diamagnetic drifts.⁵⁰ Later work showed that at large viscosity the island poloidal rotation is reduced.⁵¹ In the presence of micro-instabilities, the island poloidal propagation is related to the island width $W = w/\rho_i$.⁵ Kinetic theory of TM predicts mode growth for positive tearing parameter Δ' and rotation in the electron diamagnetic drifts direction during its linear evolution.^{52–54}

Here we address the rotation of the tearing in mode in both its linear and nonlinear phase. We show that the linear phase is usually characterized by a rotation in the electron diamagnetic direction, as expected, unless the ion temperature gradient dominates the others. A reversal from electron to ion direction is usually observed at the transition from the linear to the saturated phases. The generation of an electro-

static potential that forces the electrons to co-rotate with the island is observed, as expected from previous theoretical and numerical results.^{43,55,56}

The paper organization is as follows. In Sec. (II) we briefly describe the ORB5 code and the tearing mode initialization. In Sec. (III), we compare linear simulations results for flat density and temperature profile to kinetic and two-fluids theoretical model (Sec. (III A)) while the nonlinear evolution of the tearing mode and the island-induced turbulence at its separatrix are investigated in Secs. (III B)-(III D). Sec. (IV) discuss the impact of finite temperature and density gradients on the linear and nonlinear tearing mode evolution. The linear tearing mode growth and frequency are investigated in Secs. (IV A)-(IV B) while Sec. (IV C) discusses the nonlinear island rotation frequency and its relation to the $\mathbf{E} \times \mathbf{B}$ flow for gradients that are kept below the linear threshold for micro-instabilities. A summary of our results is given in Sec. (V).

II. ORB5 CODE

A. Physics Model

We make use of the ORB5 code which is a global gyrokinetic particle-in-cell (PIC) code that solves the gyrokinetic Vlasov-Maxwell system of equations.⁵⁷ ORB5 uses the mixed-variable formulation of the gyrokinetic formulation which splits the electromagnetic potential into a symplectic and a Hamiltonian part $A_{\parallel} = A_{\parallel}^{(s)} + A_{\parallel}^{(h)}$.⁵⁸ The species distribution function f_s is split into a background distribution variate F_{0s} , chosen as a shifted Maxwellian, and a time-dependent deviation from it δf_s : $f_s = F_{0s} + \delta f_s$ for species s (bulk plasma ion or electrons). The distribution function F_{0s} can be used as a control variate to reduce the sampling noise. The evolution of δf_s is obtained solving the gyrokinetic Vlasov equation

$$\frac{\partial \delta f_s}{\partial t} + \dot{\mathbf{R}} \cdot \frac{\partial \delta f_s}{\partial \mathbf{R}} + v_{\parallel} \frac{\partial \delta f_s}{\partial v_{\parallel}} = -\dot{\mathbf{R}}^{(1)} \cdot \frac{\partial F_{0s}}{\partial \mathbf{R}} - v_{\parallel}^{(1)} \frac{\partial F_{0s}}{\partial v_{\parallel}}, \quad (1)$$

Markers, or numerical particles, evolve accordingly to the gyrokinetic evolution equation for the gyrocenter \mathbf{R} and the

velocity parallel to the equilibrium magnetic field v_{\parallel}

$$\dot{\mathbf{R}} = \dot{\mathbf{R}}^{(0)} + \dot{\mathbf{R}}^{(1)}, \quad v_{\parallel} = v_{\parallel}^{(0)} + v_{\parallel}^{(1)} \quad (2)$$

$$\dot{\mathbf{R}}^{(0)} = v_{\parallel} \mathbf{b}_0^* + \frac{1}{q_s B_{\parallel}^*} \mathbf{b} \times \mu \nabla B, \quad v_{\parallel}^{(0)} = -\mu \mathbf{b}_0^* \cdot \nabla B \quad (3)$$

$$\dot{\mathbf{R}}^{(1)} = \frac{\mathbf{b}}{B_{\parallel}^*} \times \nabla \langle \phi - v_{\parallel} (A_{\parallel}^{(s)} + A_{\parallel}^{(h)}) \rangle - \frac{q_s}{m_s} \langle A_{\parallel}^{(h)} \rangle \mathbf{b}^* \quad (4)$$

$$v_{\parallel}^{(1)} = -\frac{q_s}{m_s} \left[\mathbf{b}^* \cdot \nabla \langle \phi - v_{\parallel} A_{\parallel}^{(h)} \rangle + \frac{\partial}{\partial t} \langle A_{\parallel}^{(s)} \rangle \right] - \mu \frac{\mathbf{b} \times \nabla B}{B_{\parallel}^*} \cdot \nabla \langle A_{\parallel}^{(s)} \rangle \quad (5)$$

$$\mathbf{b}^* = \mathbf{b}_0^* + \frac{\nabla \langle A_{\parallel}^{(s)} \rangle \times \mathbf{b}}{B_{\parallel}^*}, \quad \mathbf{b}_0^* = \mathbf{b} + \frac{m_s v_{\parallel}}{q_s B_{\parallel}^*} \nabla \times \mathbf{b} \quad (6)$$

$$B_{\parallel}^* = B + \frac{m_s v_{\parallel}}{q_s} \mathbf{b} \cdot \nabla \times \mathbf{b} \quad (7)$$

The superscript (0) and (1) indicate the unperturbed and perturbed variables and the gyro-average $\langle \zeta \rangle = \oint \zeta(\mathbf{R} + \boldsymbol{\rho}) d\alpha / (2\pi)$ for $\zeta = \phi, A_{\parallel}$ with $\boldsymbol{\rho}$ the gyro-radius of the particle and α the gyro-phase. The symbol $\mu = m_s v_{\perp}^2 / (2B)$ is the magnetic moment, m_s the particle mass, $\mathbf{b} = \mathbf{B}/B$ with $B = |\mathbf{B}|$ and $\langle \phi \rangle$ is the perturbed electrostatic potential. The Ohm's law is written for the symplectic part of the electromagnetic potential⁵⁸

$$\frac{\partial}{\partial t} A_{\parallel}^{(s)} + \mathbf{b} \cdot \nabla \phi = 0, \quad (8)$$

and the field equations are

$$-\nabla \cdot \left(\frac{n_0}{B \omega_{ci}} \nabla_{\perp} \phi \right) = \sum_{s=i,e} q_s \bar{n}_{1,s} \quad (9)$$

$$\sum_{s=i,e} \frac{\beta_s}{\rho_s^2} A_{\parallel}^{(h)} - \nabla_{\perp}^2 A_{\parallel}^{(h)} = \mu_0 \sum_{s=i,e} \bar{J}_{\parallel 1,s} + \nabla_{\perp}^2 A_{\parallel}^{(s)}, \quad (10)$$

with $\omega_{ci} = q_i B / m_i$ the ion cyclotron frequency, $\rho_s = \sqrt{m_i T_e} / (q_i B)$ the species sound thermal gyro-radius, $q_s = e Z_s$ (Z_s the atomic number, e the elementary charge) the species charge, $\beta_s = \mu_0 q_s n_s T_s / B_0^2$ the ratio of kinetic to magnetic pressure for species s , $\bar{n}_{1,s} = \int d^6 Z \delta f_s \delta(\mathbf{R} + \boldsymbol{\rho} - \mathbf{x})$ and $\bar{J}_{\parallel 1,s} = \int d^6 Z v_{\parallel} \delta f_s \delta(\mathbf{R} + \boldsymbol{\rho} - \mathbf{x})$ the perturbed gyro-center density and parallel current with $d^6 Z = B_{\parallel}^* d\mathbf{R} dv_{\parallel} d\mu d\alpha$ the phase-space volume. In our simulations, the electron parallel flow is much smaller than the thermal speed and the deviation of the shifted Maxwellian, with respect to equilibrium, is in the range 1.14 to 0.011 $c_s = \sqrt{T_e / m_i} \cong v_{th,i} \ll v_{th,e}$. There is no significant deviation of the marker distribution compared to the distribution used in the derivation of the weight equation.

Electromagnetic simulations in global gyrokinetic simulations suffer from the cancellation problem.^{59,60} This problem is addressed in ORB5 solving the equations using a control variate mitigation technique and a Pullback algorithm for the mixed-variables.^{58,61–63} In ORB5, all physical variables are normalized to the following four quantities: m_i and $q_i = e Z_i$ the ion mass and charge, the magnetic field amplitude at the

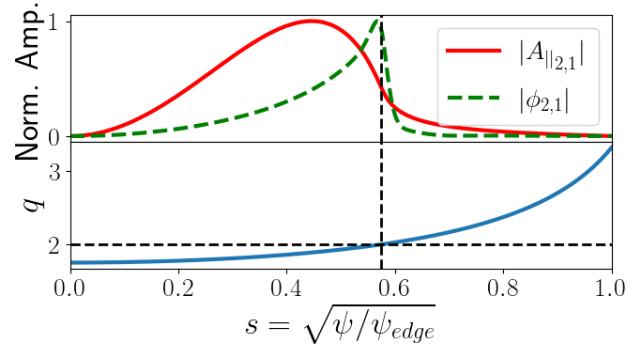


Figure 1 – Radial profiles of $|A_{\parallel 2,1}|$ and $|\phi_{2,1}|$ for an unstable tearing mode in toroidal geometry and safety factor profile q . The vertical dashed line indicates the radial position of the $q = 2$ resonant surface.

magnetic axis B_0 and the electron temperature $T_e(s_0)$ at a reference magnetic surface s_0 .⁵⁷ In addition, the volume average electron density $\langle n_e \rangle$ is a fifth normalised quantity used in the electromagnetic version of the code. The normalized radial coordinate is given by $s = \sqrt{\psi/\psi_{edge}}$ using the initial equilibrium geometry. Finally, all species are treated kinetically, the ions gyrokinetically, and the electrons drift-kinetically, without fast particles, for the tearing mode simulations described below.

B. Definition of Linear Simulations in ORB5

The linearized Vlasov equation Eq. (1) is written as

$$\frac{\partial \delta f_s}{\partial t} + \dot{\mathbf{R}}^{(0)} \cdot \frac{\partial \delta f_s}{\partial \mathbf{R}} + v_{\parallel}^{(0)} \frac{\partial \delta f_s}{\partial v_{\parallel}} = -\dot{\mathbf{R}}^{(1)} \cdot \frac{\partial F_{0s}}{\partial \mathbf{R}} - v_{\parallel}^{(1)} \frac{\partial F_{0s}}{\partial v_{\parallel}} \quad (11)$$

The left-hand-side is the Lagrangian derivative of δf along the unperturbed trajectories while the right-hand-side (rhs) depends on the perturbed potentials. Linear simulations can be performed evolving the system along unperturbed trajectories by evaluating the rhs at the new particle position at each time step.

C. Tearing Mode Initialization

In ORB5, the Maxwellian distribution function of the electrons can be shifted such that it is not centered around $v_{\parallel} = 0$ and produces an equilibrium electron flow consistent with the desired equilibrium current. In such a case, the electron bulk velocity is obtained as $v_{\parallel,0} = -J_{\parallel} / (en_e)$, where the equilibrium parallel current density J_{\parallel} is calculated from the background magnetic field \mathbf{B} as $J_{\parallel} = \mathbf{b} \cdot \nabla \times \mathbf{B}$, with $\mathbf{b} = \mathbf{B}/|\mathbf{B}|$. The tearing mode is destabilized initializing a safety factor q profile obtained from the Wesson analytic

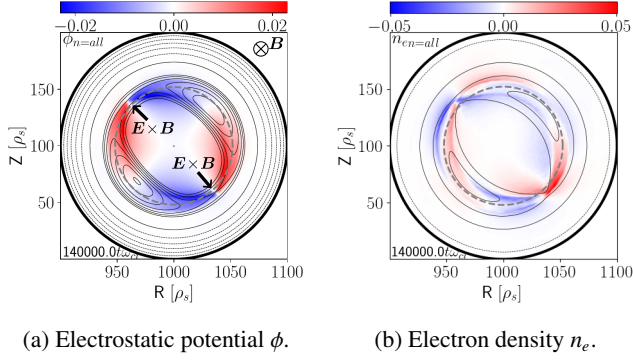


Figure 2 – Poloidal cross sections showing the tearing mode structures of normalised (a) electrostatic potential ϕ and (b) electron density n_e . The potential leads to $\mathbf{E} \times \mathbf{B}$ inflows towards the X-points.

form of the following current density profile⁶⁴

$$J_{\parallel} = J_0 \left(1 - \left(\frac{r}{a} \right)^2 \right)^{\zeta}. \quad (12)$$

Here J_0 is the current on axis, r the radial position, a the location of the current peaking on r and ζ an integer determining the peaking of the current. In our simulations, $\zeta = 1$. The safety factor q -profile associated to this current is

$$q = q_a \frac{r^2/a^2}{1 - (1 - r^2/a^2)^{\zeta+1}}, \quad (13)$$

with $q_a = q(r = a)$ and the on-axis value $q_0 = q(r = 0)$. In our simulations, we choose $q_0 = 1.75$ and $q_a/q_0 = \zeta + 1 = 2$. The initial safety factor q profile condition destabilizes a tearing mode with helicity $(m, n) = (2, 1)$ at radial position $s = \sqrt{\psi/\psi_{edge}} = 0.57$. Fig. 1 shows the profiles of the electrostatic potential $|\phi|$, the parallel component of the potential vector $|A_{\parallel}|$ and the safety factor q with respect to the normalized radial direction $s = \sqrt{\psi/\psi_{edge}}$. The vertical dashed-line shows the resonant surface $q = 2$ where the tearing mode is current unstable. The profiles are taken at the time the tearing mode has established its linear growth. The tearing parameter for this profile is $\Delta' = 21.3$.

Finally, we consider a circular cross-section tokamak with a minor radius, in Larmor units $\rho_i = m_i v_{th,i}/eB$, given by the parameter $lx = 2a/\rho_s = 200$, a mass ratio $m_i/m_e = 1/0.005 = 200$ and aspect ratio $\varepsilon = a/R_0 = 0.1$ for a minor radius $a = 1$ [m] and major radius (at plasma center) $R_0 = 10$ [m]. The magnetic field on axis $B_0 = 1$ [T]. The number of grid points are $(n_s, n_{\phi} = 128, n_{\chi} = 384)$, where n_s , n_{ϕ} and n_{χ} are the radial, toroidal and poloidal directions. The Fourier decompositions are applied to the toroidal and poloidal directions. The radial grid number ranges from $n_s = 320$ to 900 such that the electron skin depth, which depends on the plasma β and mass ratio m_i/m_e values (Eq. (15)), is always resolved by at least 5 grid points.⁶⁵ The initial load of mark-

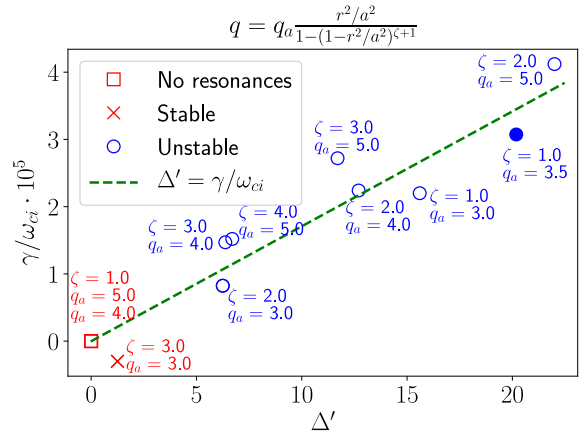


Figure 3 – Growth rate γ of the mode $m/n = 2/1$ against the tearing parameter Δ' for several parameters $\zeta = q_a/q_0 - 1$ and q_a of Eq. (13). The growth rate increases with the tearing parameter. The filled blue circle corresponds to the parameters selected for the present investigation. $\beta = 0.1\%$, $m_i/m_e = 800$.

ers are $4 \cdot 10^8$ for the ions and $8 \cdot 10^8$ for the electrons.

$$\beta_e = \frac{\mu_0 N_0 T_0}{B_0^2}, \quad (14)$$

where $N_0 = \langle n_e \rangle$ is the volume averaged electron density and $T_0 = T_e(s_p)$ at radial location s_p where the gradients are maximum. We obtain the linear evolution of the tearing mode that has a $m/n = 2/1$ helicity structure (Fig. 2a), as expected by theory.³ The figure further depicts the $\mathbf{E} \times \mathbf{B}$ inflows towards the X-points. In slab geometry, the density is localized in the X-points vicinity with a quadrupole structure.^{66,67} In toroidal geometry, such a quadrupole structure is visible around the high-field side X-point (top-left X-point). Compared to slab geometry, the quadrupole structure gets shifted and tilted at the low-field side. A more detailed analysis of the reasons for this asymmetry is left for future work. In our simulations, we use the reduced mass ratio $m_i/m_e = 200$ in order to reduce the computational costs and to be able to perform several parameter scans (we also notice that the mass ratio can be used to control the growth rate of the TM, as shown later). In Sec. (III B), we compare selected results to the more realistic mass ratio $m_i/m_e = 1600$.

III. TEARING MODE WITH FLAT TEMPERATURE AND DENSITY PROFILES

Kinetic theory of collisionless tearing mode states that the tearing mode growth rate γ depends on the plasma β as well as the mass and temperature ratio value.^{29,68} We will compare the theoretical growth rate to our simulations scanning these parameters. In ORB5, the plasma β_e is introduced in terms of the electron pressure as: In ORB5, varying β_e as an input parameter corresponds to a variation of the density,

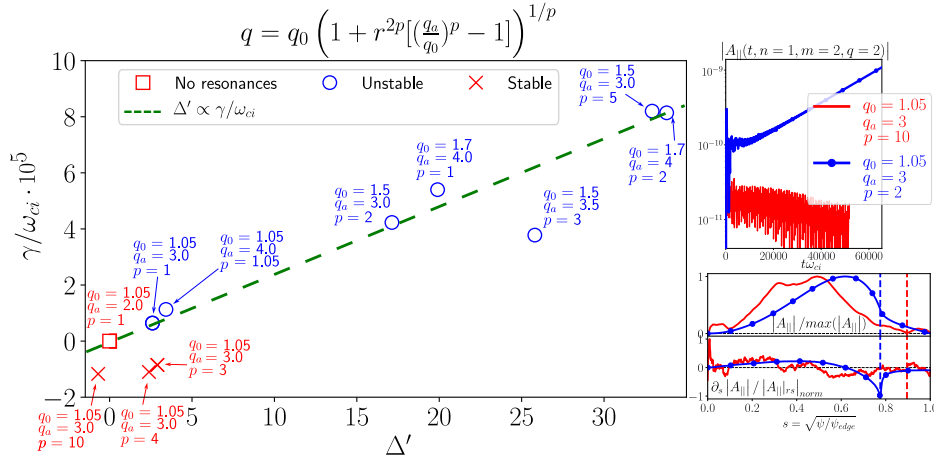


Figure 4 – Growth rate γ against the tearing parameter Δ' , for the mode $m/n = 2/1$, for several parameters q_0 , q_a and p of Eq. (17). The time trace of $A_{||}(n = 1, m = 2, q = 2)$, its radial profile and radial derivatives are shown on the right panels for a typical stable (red) and unstable case (blue). $\beta = 0.1\%$, $m_i/m_e = 400$.

which in turn implies a change in the collisionless skin depth $d_e = c/\omega_{pe}$, where $\omega_{pe}^2 = N_0 e^2/m_e \epsilon_0$ is the square of electron plasma frequency. Making use of the above definition, the electron plasma β is written as

$$\beta_e = \left(\frac{1}{d_e}\right)^2 \frac{m_e}{m_i} \rho_s^2, \quad (15)$$

In fusion plasmas, ρ_s is usually larger than the collisionless skin depth, i.e. the relevant regime is $d_e < \rho_s$. The growth rate of the tearing mode in the collisionless limit reads:²⁹

$$\gamma/\omega_{ci} = \Delta' k_\theta k_r \rho_s^3 \frac{B_\theta}{B_\phi} \left(1 + \frac{T_i}{T_e}\right)^{1/2} \left(\frac{m_e}{m_i}\right)^{1/2} \frac{1}{\beta_e}, \quad (16)$$

where Δ' is the tearing parameter,¹ $k_\theta = m/r$ is the tearing poloidal wave number, k_r is the radial wave number, B_θ and B_ϕ are the poloidal and toroidal magnetic field. The estimation is valid in the limit of small Δ' which is the relevant limit for Tokamak tearing modes with poloidal mode number $m > 1$.²⁹ Eq. (16) shows that the tearing mode growth rate in the collisionless limit is proportional to $1/\beta_e$ (or d_e^2) at fixed T_i , T_e and mass ratio. In the remaining of the paper, we use the notation $\beta \equiv \beta_e$.

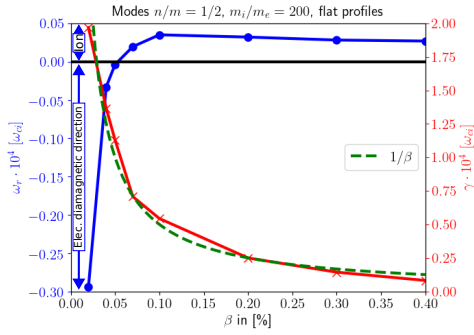
A. Linear growth of the tearing mode

We start with a code-theory comparison initializing a tearing mode at the rational surface $q = m/n = 2/1$ and performing linear simulations varying the tearing parameter Δ' , the plasma β and the mass ratio m_i/m_e for flat temperature and density profiles. The parameters have the following values, except when varied: $\beta = 0.2\%$, $m_e/m_i = 0.005$, $T_e/T_i = 1$ and $\nabla T/T = \nabla n/n = 0$. The linear simulations are performed for the toroidal mode number $n = 1$ with poloidal mode numbers in the intersection of two fil-

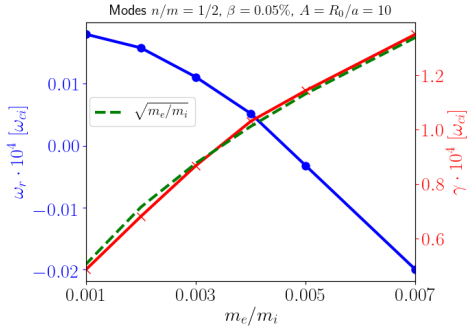
ters: a) $nq + m \leq \delta m$, with $\delta m = 5$ and b) $[-m_{max}; m_{max}]$ where $m_{max} \approx n_{max} q_{max} \approx 4$. The tearing parameter Δ' is determined by the eigenfunction of $A_{||}$ which is varied through the parameters q_a and q_0 of Eq. (12). Since we are interested in the tearing mode with $m/n = 2/1$, we restrict the parameter space to $1 \leq q_0 < 2$ and $2 < q_a < 5$. We estimate the tearing parameter Δ' by means of a shooting algorithm and plot the $m/n = 2/1$ mode growth rate versus Δ' (Fig. 3). The $m/n = 2/1$ tearing mode grows proportionally with Δ' . However, it is difficult to obtain a stable $m/n = 2/1$ tearing mode with a rational surface not too close to the boundaries with the profile of Eq. (13). For this reason, we use additionally the following safety factor profile (for our Δ' scan only)

$$q = q_0 \left(1 + (r/a)^{2p} \left[\left(\frac{q_a}{q_0}\right)^p - 1\right]\right)^{1/p}, \quad (17)$$

which exhibits less restrictions on the parameter space as the power p is not related to the ratio q_a/q_0 .⁶⁹ Using this profile, we obtain a stable $m/n = 2/1$ tearing mode due to a negative Δ' , using $q_0 = 1.0$, $q_a = 3$ and $p = 10$, (Fig. 4) which has the expected $A_{||}$ eigenfunction for a stable tearing mode in toroidal geometry.⁶ We further obtain that the mode is unstable for $q_0 = 1.7$, $q_a = 4$, $p = 4$ and marginally stable for $q_0 = 1.0$, $q_a = 3$ and $p = 1$ as already shown by a reduced set of two-fluid equations.⁶⁹ The fact that stable cases are observed for small but positive values of Δ' is a consequence of the fact that the tearing parameter does not accurately account for the tearing stability in toroidal systems with asymmetric current profiles.^{70,71} We further compare our simulations with the theoretical trends derived from Eq. (16). We obtain that the tearing mode growth rate γ decreases with an increased value of the plasma β (Fig. 5a) or mass ratio m_i/m_e (Fig. 5b) as theoretically estimated by Eq. (16). The mass ratio allows us to change the tearing drive instead of changing the tearing parameter Δ' which would require a modification



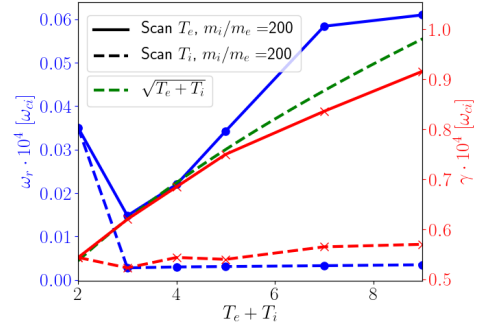
(a) Growth rate γ (red line with crosses) and frequency ω_r (blue line with circles) versus β .



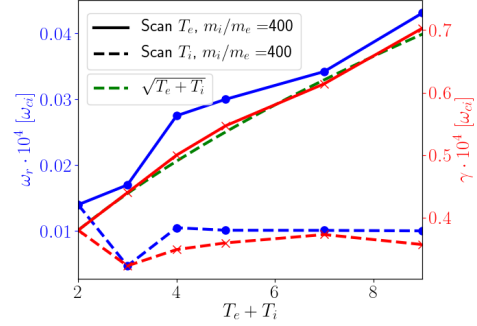
(b) Growth rate γ (red line with crosses) and frequency ω_r (blue line with circles) versus mass ratio m_e/m_i .

Figure 5 – Tearing mode linear simulations ($n = 1$) for flat temperature and density profiles. (a): The $1/\beta$ scaling (Eq. (16)) of the $A_{\parallel 2,1}$ growth rate γ is obtained for $\beta < 0.4\%$ (cf. discussion in Sec. (IV A)). The tearing mode has a weak rotation frequency ω_r whose sign depends on β . Electron diamagnetic drift direction for $\omega_r < 0$. (b): The mode growth rate γ decreases as the electron mass is reduced. In both plots, the green dashed-line represents the theoretical scaling.

of the safety factor profile q .⁷² But, changing the q profile might lead to several rational surface where the tearing mode is unstable, a situation we want to avoid in order to investigate the nonlinear evolution of the tearing mode at a single rational surface. Finally, we scan the temperature ratio. We obtain the expected scaling, $\gamma \propto \sqrt{T_i + T_e}$, when changing the electron temperature T_e , while it is much weaker when T_i is varied (Fig. 6). This gyrokinetic behavior was already observed previously and associated to the limitation of the model for $m_e/m_i < \beta$.²⁹ Good agreement was reported at much higher values of the mass ratio.³⁰ Fig. 1, Fig. 5 and Fig. 6 show that our initialization provides a physically consistent $m/n = 2/1$ tearing mode. Furthermore, a successful benchmark with the GENE code,^{30,73} in which a shifted Maxwellian for the electrons and for the ions were recently implemented, showed also a good agreement.²⁷ A small but finite rotation frequency of the tearing mode of the order of $10^{-6}\omega_{ci}$ is observed as the plasma β is varied (Fig. 5a). In our normalization, a negative frequency corresponds to a rota-



(a) Temperature scan, $m_i/m_e = 200$



(b) Temperature scan, $m_i/m_e = 400$.

Figure 6 – Scans in temperatures for (a) mass ratio $m_i/m_e = 200$ and (b) $m_i/m_e = 400$. Good agreement of the growth rate γ (red curves) with theoretical scaling $\sqrt{T_e + T_i}$ is obtained for T_e scans. The disagreement with theoretical scaling changing T_i is related to the limitations of the theoretical model, confirming the results in Pueschel *et al.*³⁰

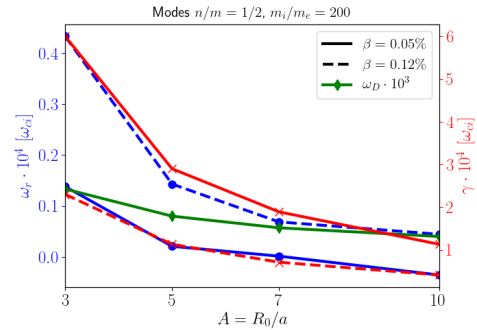


Figure 7 – Growth rate γ and real frequency ω_r (< 0 electron diamagnetic drift direction) versus the aspect ratio $A = R_0/a$, flat density and temperature profile. Increasing A reduces γ and ω_r . The frequency is negative at $\beta = 0.05\%$ and $A = 10$. The magnetic drift $\omega_D^* = -k_\theta T_0 / (eB_0) \nabla B \times B / B^2$ is represented in green.

tion in the electron diamagnetic direction. The mode rotates in the electron diamagnetic direction⁷⁴ for $\beta < 0.07\%$ and in the ion diamagnetic drift direction otherwise. The mode rotation decreases as the mass ratio is increased at fixed β . This weak rotation of the mode for flat temperature and density profiles has been ascribed to toroidicity effects,⁷² but its dependence on β was not investigated. Finite magnetic field gradient lead to a grad-B drift $\omega_D^* = -k_\theta T_0 / (eB_0) \nabla B \times B / B^2$ due to circular cross-section. A two-fluid model gives the relation $\omega_{TM} \cong \omega_n^* + \alpha \omega_T^* + \omega_{E \times B} + \omega_D^* + \omega_\eta^*$, where ω_{TM} is the tearing frequency, ω_n^* and ω_T^* the density and temperature diamagnetic drift frequencies, α a ions species dependent parameter (hydrogen, deuterium, ...), $\omega_{E \times B} = E \times B / (B^2 r)$ the zonal flow frequency, ω_D^* the grad-B drift and ω_η^* a resistivity related drift.⁴⁸ For our parameters, the linear rotation frequency can be estimated as $\omega_{TM} \cong \omega_D^*$. Fig. 7 shows that the growth rate and the frequency decrease for larger aspect ratios $A = R/a$ as $\gamma \propto (1 + 2/A)$.²⁶ Removing the mirror force from the electron dynamics, shows that the contribution of the trapped electron population to the growth rate, for our Δ' , is weak a low A and negligible at large A . The frequency of the tearing mode is reduced in presence of trapped electrons. Still, the frequency decreases with increasing A . We conclude that the weak rotation frequency of the tearing mode is related to curvature effects and the plasma β .

B. Nonlinear Island Decay

We perform nonlinear simulations with flat density and temperature profiles, allowing for the back reaction of the perturbed fields on the particles trajectories (excluded in the linear simulations presented in the previous section), using $n \in [0, 30]$, with $n \in \mathbb{N}$, toroidal modes. The poloidal modes are $m \in [nq - 5, nq + 5]$, with $m \in \mathbb{Z}$, as explained in Sec. (II C). The time evolution of the island width for three values of the plasma β are compared in Fig. 8. These simulations have an unstable tearing mode whose linear growth reduces with increasing plasma β as $1/\beta$ (Eq. (16)). The magnetic island width is $W = w/\rho_s = \sqrt{2q|A_{||2,1}|}/s$, with s the normalised magnetic shear length and $\rho_s = \rho_i/\sqrt{2}$.⁷⁵ Since the time evolution of $A_{||2,1}$ is in arbitrary units, the island width can be computed as $W = C \sqrt{|A_{||2,1}|}$ with a conversion factor $C = 626.68$. The maximum island size is observed to diminish as the linear growth reduces. After the peak in the island size, the island evolution differs depending on β . At the lowest value $\beta = 0.05\%$, a strong decay of the island size W is observed after its peak which is then followed by a weaker decrease. This island size reduction process weakens as the tearing drive is reduced by increasing β . In particular, for $\beta = 0.12\%$ there is almost no island decay after the maximum amplitude is reached, and the island saturation size is similar to that obtained after a weak island decay for $\beta = 0.07\%$ (Fig. 8). Due to this nonlinear decay process, there are no direct correlations between the tearing linear growth and the island size at the quasi-steady state. However, a strongly driven tearing mode impacts the

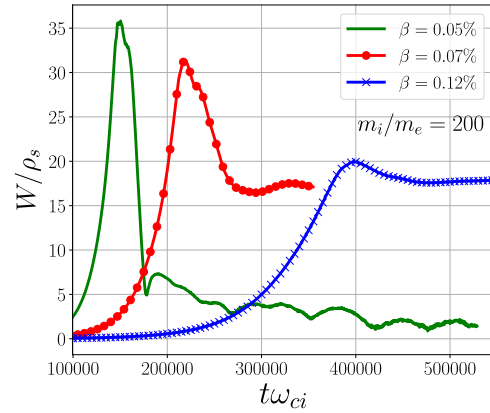


Figure 8 – Time evolution of the normalised magnetic island width W , for different values of β_e with mass ratio $m_i/m_e = 200$.

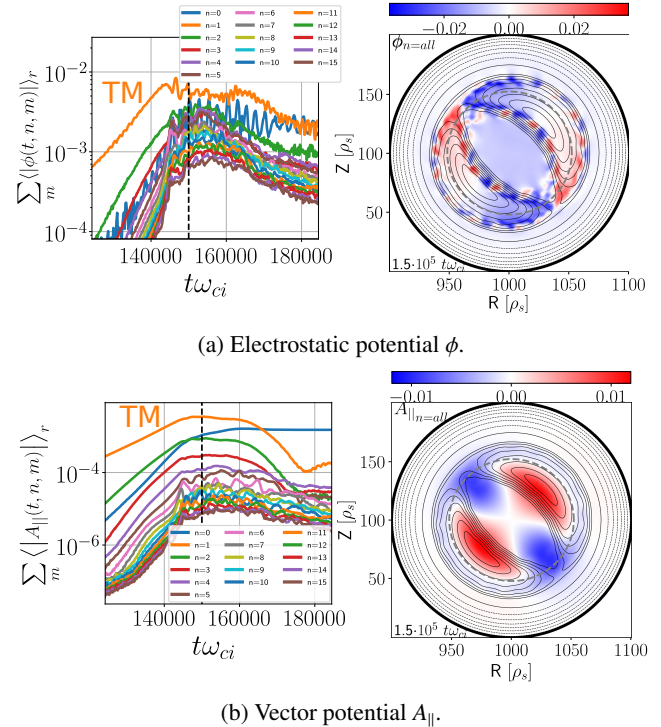


Figure 9 – Time evolution of the toroidal mode amplitudes, summed over the poloidal modes and averaged over the radius, and poloidal cuts for normalised (a) ϕ and (b) $A_{||}$ including all toroidal modes. The vertical dashed line corresponds to the time of the contour plots. Plasma $\beta = 0.05\%$ and $m_i/m_e = 200$.

maximum size that the island can reach before the beginning of the decay process. The temporal evolution of the toroidal Fourier amplitudes of ϕ and $A_{||}$, averaged over the radius, and poloidal cuts of the potentials for $\beta = 0.05\%$ and 0.12% are depicted in Figs. 9-10. As the island reaches its maximum size, strong electrostatic turbulence is produced at the island separatrix and strong zonal currents ($A_{||n=0}$) de-

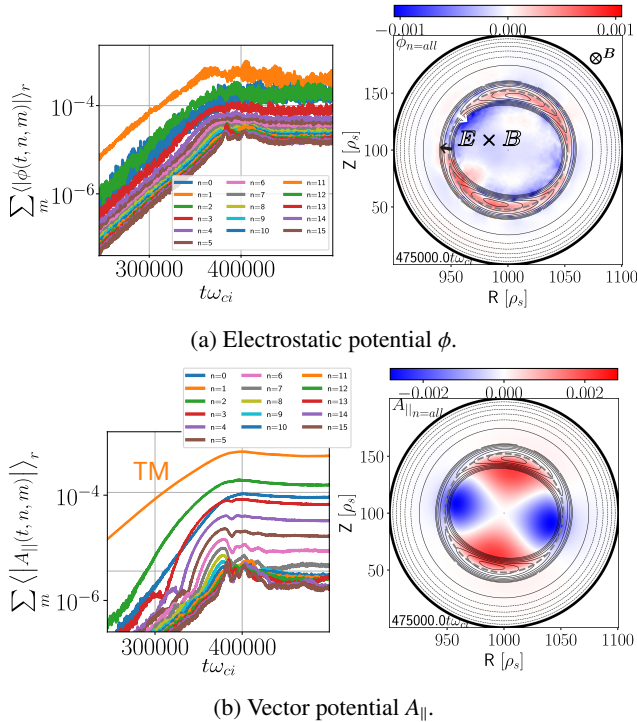


Figure 10 – Time evolution of the toroidal mode amplitudes, summed over the poloidal modes and averaged over the radius, and poloidal cuts for normalised (a) ϕ and (b) $A_{||}$ including all toroidal modes. The contour plots are taken at the simulation end. Plasma $\beta = 0.12\%$ and $m_i/m_e = 200$.

velop when the island decay process begins for $\beta = 0.05\%$ (Fig. 9b left). Oppositely, much weaker zonal currents are produced and almost no turbulence develops for $\beta = 0.12\%$ (Fig. 10b). Two mechanisms seem to be at play for the nonlinear evolution of the island: I) current density redistribution and II) nonlinear electrostatic instabilities at the island separatrix. We investigate the physics of the island decay process for $\beta = 0.05\%$ comparing the island evolution by a) decreasing the electron mass m_e by a factor of 8, b) filtering out toroidal mode number larger than $n \in [0, 2]$, and c) removing the mirror force setting the time derivative of the unperturbed parallel velocity (Eq. (3), right) for the electrons to zero (Fig. 11). We observe no decay when the electron mass is reduced ($m_i/m_e = 1600$), a small island decay process using $n \in [0, 2]$, and a moderate decay removing the mirror force (MF = 0). This behavior is discussed in Sec. (III D). We address the current redistribution first.

C. Current Redistribution and Island Size Reduction.

In the presence of large magnetic islands, strong zonal fields $A_{||}(m = 0, n = 0)$ develop when toroidal modes up to 30 are retained in the simulation. Their drive occurs at twice the growth rate of the dominant tearing instability, as expected, so these fields are weaker for reduced linear growth rate of the tearing mode, for instance increasing the

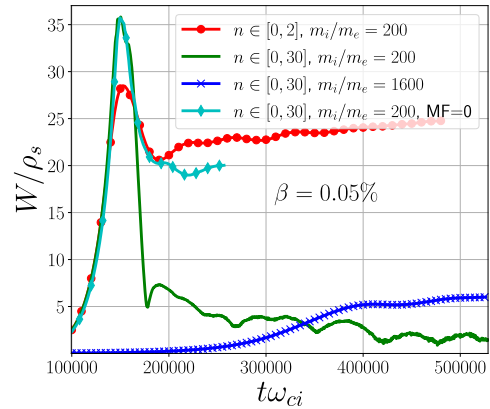


Figure 11 – Time evolution of the normalised island width W for mass ratio $m_i/m_e = 200$ and 1600 with $n \in [0, 30]$, $m_i/m_e = 200$ with $n \in [0, 2]$ and artificially removing the mirror force (MF) for $m_i/m_e = 200$ with $n \in [0, 30]$.

plasma β or reducing the electron mass m_e . The zonal magnetic fields are found to impact the island evolution through the modification of the background current density $J_{||}$ and the safety factor q profile. Fig. 12 compares the modification of these profiles for simulations with $\beta = 0.05\%$, $n \in [0, 2]$ (red curve) and $[0, 30]$ (green curve) with mass ratio $m_i/m_e = 200$, $n \in [0, 30]$ with $m_i/m_e = 1600$ (blue curve) and $n \in [0, 30]$ with $m_i/m_e = 200$ setting the mirror force (MF) for the electrons to zero (cyan curve). While in the case $m_i/m_e = 1600$ the island saturates at a quite low level, see Fig. 11, with no visible modification of the current profile, a clear flattening of the radial current profile is obtained for $m_i/m_e = 200$. The radial range of the flattening is quite broad if toroidal modes up to 30 are retained and does not seem to be influenced by the presence (or absence) of trapped electrons. If only modes from 0 to 2 are retained, the island size, zonal currents and the flattening of the current profiles are reduced. The safety factor profile is modified as the island reaches its maximum width and the rational surface $q = 2$ moves from $s = 0.57$ to 0.53 , closer to the plasma center. The fact that the modification of the current profile is almost identical with and without electron trapping, together with the fact that both cases exhibit the same dynamics until the maximum island amplitude is reached, suggests that the current perturbation is the main effect stopping the island growth and initiating its decrease in these strongly-driven cases. Its further evolution is associated to the modification of the flows, which is different depending on whether the mirror force is included or not, as explained in Sec. (III D). As stated before, the growth of the zonal currents (related to the axisymmetric part of $A_{||}$) show that they are nonlinearly driven by the tearing instability and saturate with it. In other words, the current profile flattening is not a result of the excitation of the electrostatic turbulence, described in the next subsection, as it is also present for the simulation including toroidal modes 0 to 2.

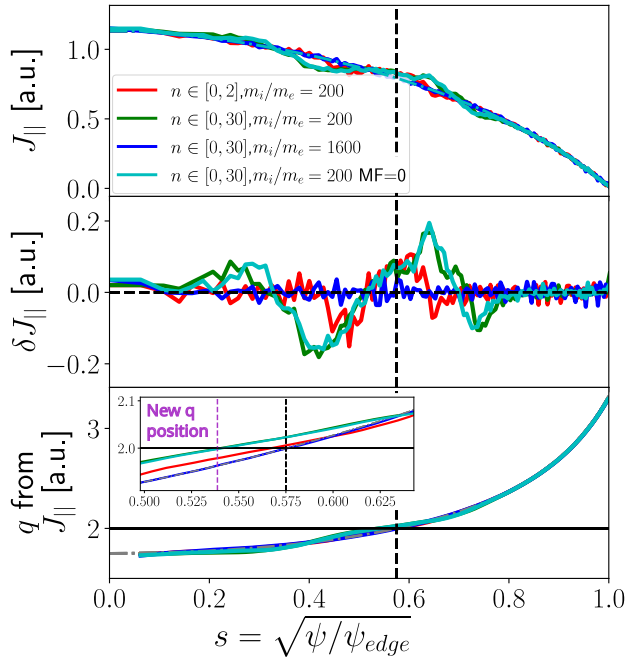
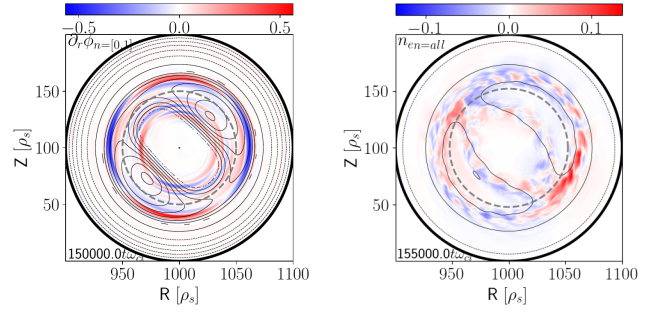


Figure 12 – Poloidally and toroidally averaged parallel current profile J_{\parallel} , its perturbation $\delta J_{\parallel} = J_{\parallel} - J_{\parallel,t=0}$ and safety factor q computed from the current profiles shortly after the islands reach their maximum size.

Red curve: $n \in [0, 2]$, $m_i/m_e = 200$ at $t\omega_{ci} = 1.55 \cdot 10^5$.
 Green curve: $n \in [0, 30]$, $m_i/m_e = 200$ at $t\omega_{ci} = 1.55 \cdot 10^5$.
 Blue curve: $n \in [0, 30]$, $m_i/m_e = 1600$ at $t\omega_{ci} = 4.1 \cdot 10^5$.
 Cyan curve: $n \in [0, 30]$, $m_i/m_e = 200$ at $t\omega_{ci} = 1.55 \cdot 10^5$ with electron mirror force (MF) set to 0. The black dashed-line represents the equilibrium $q = 2$ resonant surface.

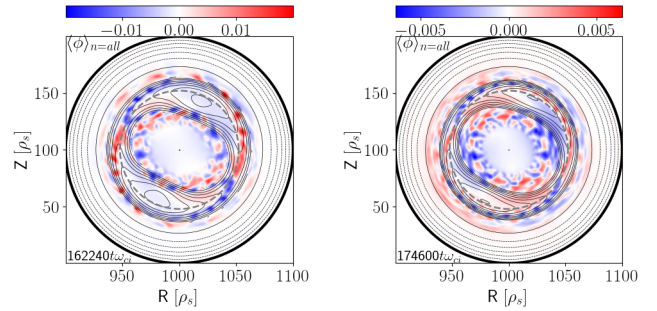
D. Kelvin-Helmholtz Instability (KHI) and Island Saturation Mechanism.

We investigate the instability at the island separatrix scrutinizing the electron density n_e and ϕ fluctuations for the case with $\beta = 0.05\%$ and $n \in [0, 30]$, including the mirror force for the electrons, shown in Fig. 9. We observe that the localized ϕ and n_e structures along the island separatrix (Fig. 2) imply strong $\mathbf{E} \times \mathbf{B}$ and diamagnetic flows, which can become unstable to the Kelvin-Helmholtz instability (KHI). Excitation of KHI has been observed before in magnetic reconnection, and particularly in collisionless reconnection with asymmetric current profiles, see e.g.^{76,77} and references therein, and in particular very recently at the separatrix of strongly driven magnetic islands.⁷⁸ Figs. 13a-13b show that the island develops strong $n = 1$ potential structure at its separatrix, before the growth of fluctuations. The related sheared flows destabilize the KHI at the island separatrix, more clearly in the inner region (between the island and the magnetic axis), as shown by the vortices in the density (Fig. 13b). Additionally, we obtained that the velocity jump across the separatrix, computed using the $\mathbf{E} \times \mathbf{B}$ flow

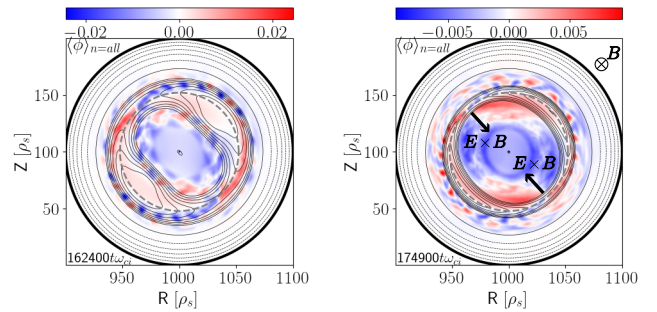


(a) Zonal ($n = 0$) plus island ($n = 1$) flows. (b) Electron density fluctuations n_e .

Figure 13 – Poloidal cross-sections representing: (a) the radial derivative of the sum of the zonal ($n = 0$) and island-related ($n = 1$) components of the normalised electrostatic potential, exhibiting a dominant $m/n = 2/1$ helicity at the separatrix and (b) the normalised electron density fluctuations n_e showing vortex flow similar to the Kelvin-Helmholtz instability, particularly visible in the inner region. Plasma $\beta = 0.05\%$ and $m_i/m_e = 200$.



(a) $t\omega_{ci} \in [1.6, 1.65] \cdot 10^5$ MF = 0 (b) $t\omega_{ci} \in [1.65, 1.85] \cdot 10^5$ MF = 0



(c) $t\omega_{ci} \in [1.6, 1.65] \cdot 10^5$ MF \neq 0 (d) $t\omega_{ci} \in [1.65, 1.85] \cdot 10^5$ MF \neq 0

Figure 14 – Time averaged of the normalised electrostatic potential $\langle \phi \rangle$ for $\beta = 0.05\%$, $n \in [0, 30]$ and $m_i/m_e = 200$. Top line: without mirror force MF = 0. Bottom line: with mirror force MF \neq 0. (d): Turbulence structures are merged into larger ones with helicity $m/n = 2/1$. The local $\mathbf{E} \times \mathbf{B}$ outflows flows are depicted by the black arrows.

as a proxy for the velocity, is larger than the Alfvén speed, as expected for an unstable Kelvin-Helmholtz instability.⁷⁹

Since the island evolution differs starting from $t\omega_{ci} \cong 1.7 \cdot 10^5$ retaining the mirror force or not, we investigate in what manners the electrostatic turbulence changes in the presence (or absence) of trapped particles. Fig. 14 depicts the time average of the electrostatic potential over $t\omega_{ci} \in [1.6, 1.65] \cdot 10^5$ and $[1.65, 1.85] \cdot 10^5$. A much stronger $n = 1$ component of ϕ can be observed when electron trapping is retained. The associated $\mathbf{E} \times \mathbf{B}$ flows correspond to a shrinking of the magnetic island, as they point away from the island X-point, as can be checked by a comparison with the flows during the growing phase of the island shown in Fig. 2a, resulting in the reversed reconnection. Without the mirror force, the $n = 1$ vortices are weaker, the higher- n turbulent structures persist and dominate the flow dynamics. Because the nature of turbulence is different with and without trapped electrons, we investigate the amplitude of the toroidal modes, summed over poloidal modes, and averaged separately over the inner and outer regions, i.e., for $s \in [0.15, 0.57]$ and $s \in [0.57, 0.85]$ respectively (Fig. 15), at $t\omega_{ci} = 1.6 \cdot 10^5$, $1.65 \cdot 10^5$ and $1.75 \cdot 10^5$. In the inner region, the amplitude of $\phi_{n=0,1}$, corresponding to the zonal and island generated flows, remain about the same during the rapid island decay phase when the mirror force is included, while they decrease after the island maximum size if electron trapping is excluded (Figs. 15a-15b). The reduced flows without the mirror force seem to be related to the peak around $n = 5$ for ϕ , likely due to KHI driven turbulence, which almost disappear in time when the mirror force is included. This is clearly visible in Figs. 14c-14d, where turbulent structures persist without the mirror force.

In the outer region, additional modes peaking at $n = 10, 13$ and 19 , whose intensity reduces in time, are visible in presence of the trapped electrons populations (MF $\neq 0$) (Fig. 15c). Without the mirror force, the amplitude of $\phi_{n=1}$ drops significantly while the amplitude of $\phi_{n=0}$ increases, indicating that the island-induced flows are not enhanced. In comparison, the $\mathbf{E} \times \mathbf{B}$ flows for $\beta = 0.12\%$ ($n \in [0, 30]$) in the saturated phase seem to compensate around the low-field-side X-point while no in- or out-flows are observed at the high-field-side one (Fig. 10a right panel). The trapped electrons driven instability and KHI are less destabilized for this weaker driven tearing mode due to larger plasma β , due to the reduced size of the potential and density perturbations in this case. The results reported in this section might be relevant to the evolution of strongly-driven magnetic islands, as they develop for instance during sawtooth reconnection. This point is further addressed in the Conclusions. Here, the nonlinear flow dynamics is found to be responsible for a violent shrinking of the island, which is particularly strong in the presence of trapped electrons. A discussion of the differences in the nonlinear energy exchange processes with and without electron trapping, which would require dedicated code diagnostics that are presently not available, is left for future work.

We conclude that combination of current density redistribution by strongly driven tearing mode, the mutual interaction of the grown island with island-generated Kelvin-

Helmholtz turbulence and the trapped electrons driven instability is responsible for the island decay. These effects are weakened as the tearing mode growth rate is decreased either reducing the electron mass m_e or increasing the plasma β . Another reduction of the tearing mode can be obtained for non-flat profiles of the temperature or the density.

IV. TEARING MODE WITH TEMPERATURE AND DENSITY GRADIENTS

In this section, we investigate the evolution of the drift-tearing-mode including finite density and temperature gradients. In such a case, kinetic theory predicts that the real frequency of the tearing mode should be in electron diamagnetic drift direction for finite density gradient.⁵² The rotation direction can change depending on the ratio T_i/T_e .⁸⁰ For hot ions, the frequency was numerically obtained to be in the ion diamagnetic drift direction.⁸¹ In this section, the linear tearing mode growth rate and frequency, as well as the island frequency during the nonlinear phase, are investigated including finite temperature and density gradients. Here, the gradients are the drive of the tearing mode rotation and the contribution of ω_D (see Fig. 7) is negligible.

A. Linear Growth of the Tearing Mode

We perform first simulations scanning the temperature gradients of both species simultaneously ($\nabla T_e/T_e = \nabla T_i/T_i \equiv \nabla T/T$), for flat equilibrium density and for two values of the plasma β and an inverse aspect ratio $A = R_0/a = 10$. At $\beta = 0.05\%$, the mode growth γ is reduced increasing the temperature gradient while the real frequency increases in absolute value. The tearing frequency follows the kinetic estimation $\omega_{TM} = \omega_n^* + 0.5\omega_{T_e}^*$ and the pressure gradient has a stabilizing effect on the mode growth. A different situation is however observed for $\beta = 0.2\%$. While the growth rate γ decreases with an increased pressure gradient for $-R_0\nabla T/T < 5$ with a frequency $\omega_{TM} \cong \omega_n^* + 0.5\omega_{T_e}^*$, the growth rate increases for larger values of the normalized logarithmic gradient and the frequency deviates from $\omega_n^* + 0.5\omega_{T_e}^*$ (Fig. 16). The tearing frequency ω_{TM} remains, however, in the electron diamagnetic drift frequency ($\omega_{TM} < 0$) for the selected gradients and β values. The (very small) positive frequency at zero gradient is related to the value of the plasma β and aspect ratio ($> 0.07\%$, see Sec. (III A)). We will show in Sec. (IV B) that increasing the pressure gradient not only stabilizes the tearing mode, but equally leads to the destabilization of a pressure gradient driven mode at high plasma β . We next isolate the temperature gradient contributions of each species on the tearing mode growth rate and real frequency using $\nabla T_i/T_i \neq \nabla T_e/T_e$. Fig. 17a shows that the tearing mode rotates in the ion diamagnetic drift direction ($\omega_{TM} > 0$) when $\nabla T_i/T_i \neq 0$ and $\nabla T_e/T_e = 0$, while it drifts in the electron diamagnetic drift direction ($\omega_{TM} < 0$) when $\nabla T_i/T_i = 0$ and $\nabla T_e/T_e \neq 0$. It can be clearly seen that the electron temperature gradient has a stronger impact on the rotation as compared to the ion temperature gradient,

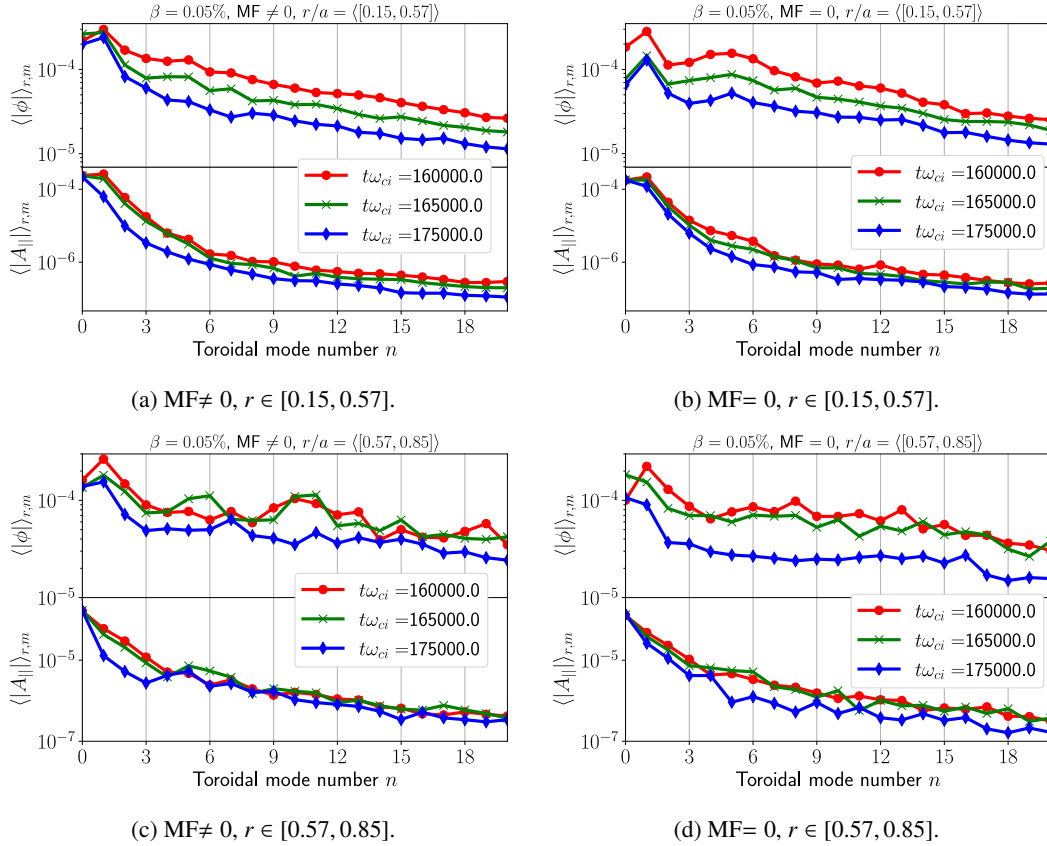


Figure 15 – Poloidal and partial radial average amplitudes for ϕ and A_{\parallel} showing the spectra for the inner region $s = [0.15, 0.57]$ when the electron mirror force MF is (a) included in electron dynamics (MF $\neq 0$) and (b) excluded (MF = 0). The spectra for the outer region $s = [0.57, 0.85]$ is shown for (c) MF $\neq 0$ and (d) MF = 0.

so that the rotation is in the electron diamagnetic direction if both gradients are equal. The tearing growth rate is decreased by both $\nabla T_e/T_e$ and $\nabla T_i/T_i$.

The role of β is illustrated on Fig. 18. The $m/n = 2/1$ mode growth follows the $1/\beta$ scaling until it grows again beyond a given threshold in β . This threshold decreases as the temperature gradient is increased. As observed for flat profiles, the mode frequency reduces in absolute value with increasing plasma β . For $-R_0 \nabla T_e/T_e = 15$, it rapidly slows down, deviating from the electron diamagnetic frequency $\omega_e^* \cong -4.5 \cdot 10^{-4} \omega_{ci}$, but remains in the electron diamagnetic drift direction (here $\nabla T_i/T_i = \nabla n/n = 0$). A similar analysis has been performed scanning the density gradient for flat electron and ion temperatures and different values of β (not shown for the sake of brevity). Similarly to Fig. 16, a transition in growth rate and frequency of the $m/n = 2/1$ mode can be observed if the density gradient exceeds a (β -dependent) threshold. The rotation of the mode turns to the ion diamagnetic direction for large density gradients (with $\nabla T/T = 0$). This behavior is discussed in the next subsection.

B. Destabilization of the $m/n = 3/1$ Mode

In order to understand the deviation of the growth rate from the $1/\beta$ scaling and of the frequency from $\omega_{TM} = \omega_n^* + 0.5\omega_{T_e}^*$ as the pressure gradient increases, we perform a β scan for $-R_0 \nabla T/T = 4$ (same logarithmic gradient for both species) and flat equilibrium density. Fig. 19 shows that the growth rate γ decreases with β until $\beta = 0.4\%$, where the mode is stable, and increases again for higher values of β . The $m/n = 2/1$ mode frequency changes from the electron ($\omega_{2,1} < 0$) to ion ($\omega_{2,1} > 0$) diamagnetic direction. The tearing is the branch where the mode frequency is close to $0.5\omega_{T_e}^*$ while the second branch has a frequency close to $0.5\omega_{T_i}^*$. The dominant instability at the $q = 2$ rational surface is, in this case, a pressure gradient driven electromagnetic mode, with rotation frequency $\omega \cong 0.5\omega_{T_i}^*$ in the ion diamagnetic direction. Inspection of the radial structures of the poloidal modes for the toroidal mode $n = 1$, Fig. 19b, reveals that the $m = 2$ has a twisting (not tearing) parity in this high- β branch with $\omega_{2,1} > 0$. The amplitude of the electromagnetic potential A_{\parallel} exhibits a strong coupling of the (2, 1) component to its neighboring poloidal harmonics. In particular, the amplitude (3, 1) component is stronger than the (2, 1) component around the $q = 2$ surface. The electrostatic poten-

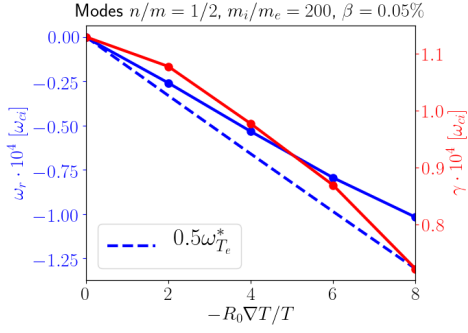
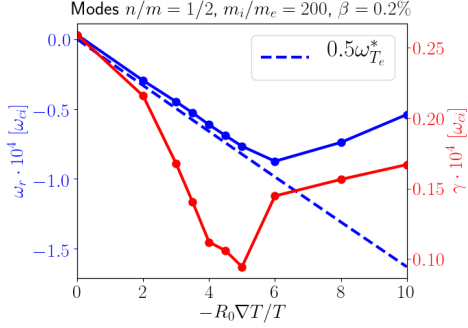
(a) $-R_0 \nabla T / T$ scan, $\beta = 0.05\%$.(b) $-R_0 \nabla T / T$ scan, $\beta = 0.2\%$.

Figure 16 – $|A_{\parallel 2,1}|$ growth rate γ and frequency ω_r versus $-R_0 \nabla T / T$ with $\nabla n / n = 0$. (a): $\beta = 0.05\%$, γ decreases with $-R_0 \nabla T / T$. The frequency ω_r is in the electron diamagnetic direction ($\omega_r < 0$), its absolute value increasing with $-R_0 \nabla T / T$. (b): $\beta = 0.2\%$, for $-R_0 \nabla T / T > 5$ an increase of the growth rate and a decrease in absolute value of the mode frequency are observed.

tial is still dominated by its (2, 1) component. Gyrokinetic simulations of collisionless tearing mode in slab geometry showed that a mode driven by a high pressure gradient, at large plasma β , can enhance the tearing mode growth rate when $\tilde{\mathbf{B}}_{\parallel}$ is non-zero.^{30,68} In such a case, the ∇B drifts are balancing the $\mathbf{E} \times \mathbf{B}$ drifts and the tearing mode is enhanced and has a rotation frequency in the ion diamagnetic drift direction. Here, the high pressure driven mode is similar but the tearing mode is stable when the pressure gradient mode is growing. In our case, the destabilization of the mode with the pressure gradient, predominantly at large plasma β , is similar to the kinetic ballooning mode (KBM) instability, so that the process resembles the well-known ITG-KBM transition with increasing β .^{82,83} Another possibility for the instability are Alfvén ion temperature gradient (AITG) modes, destabilized by pressure gradients at rational surfaces and with large frequencies in the ion diamagnetic direction.^{84,85} While additional work is required to fully understand the nature of this mode, we performed additional scans in mass ratio m_i/m_e and aspect ratio $A = R_0/a$ for $\beta = 0.8\%$ and $-R_0 \nabla T / T = 4$. The $m/n = 3/1$ mode growth rate slightly diminishes with more realistic mass ratio m_i/m_e while a larger

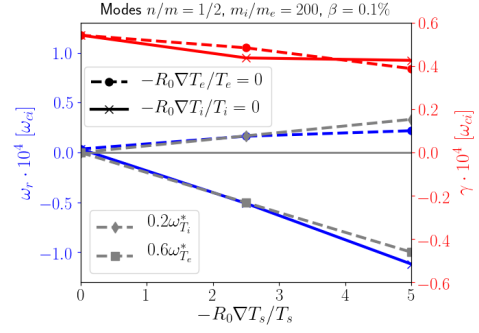
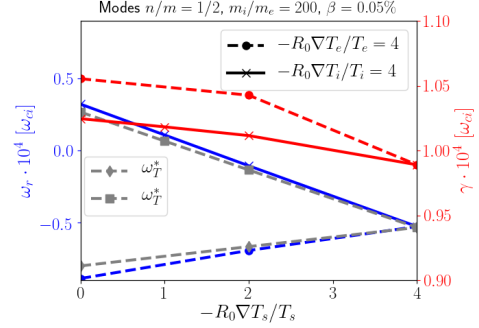
(a) Scan in $-R_0 \nabla T_s / T_s$, $s = i$ or e and $\beta = 0.1\%$.(b) Scan in $-R_0 \nabla T_s / T_s$, $s = i$ or e , $\beta = 0.05\%$ and $\omega_r^* = 0.2\omega_{T_i}^* + 0.6\omega_{T_e}^*$

Figure 17 – Tearing growth rate γ and frequency ω_r as a function of the logarithmic temperature gradient of one species (e or i), keeping the logarithmic gradient of the other species fixed either to (a) $-R_0 \nabla T / T = 0$ or (b) $-R_0 \nabla T / T = 4$.

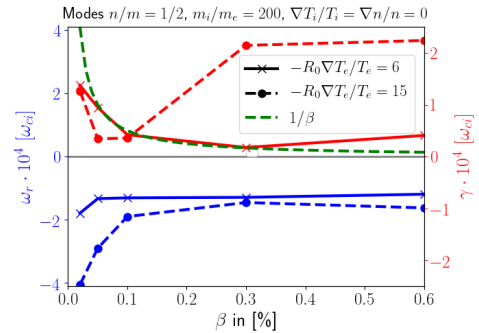


Figure 18 – Plasma β scan for $-R_0 \nabla T / T = 6$ and 15. Mode $m/n = 2/1$ growth rate γ and frequency ω_r are displayed.

The $1/\beta$ scaling is obtained for $-R_0 \nabla T_e / T_e = 6$ for $\beta \leq 0.3\%$ while the growth rate rapidly increases with β for $-R_0 \nabla T_e / T_e = 15$. The mode frequency is in the electron diamagnetic drift direction ($\omega_r < 0$), decreasing in absolute value with β .

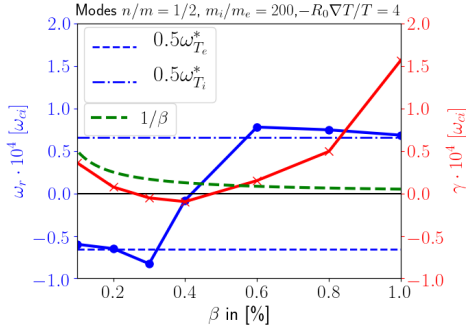
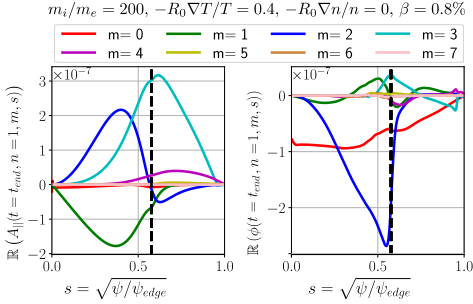
(a) Growth rate γ and frequency ω_r versus β (b) $\mathbb{R}(\phi)$ and $\mathbb{R}(A_{\parallel})$ poloidal modes radial structures of the eigenfunctions.

Figure 19 – Parameters: $\nabla n/n = 0$, $\nabla T/T = 0.4$, $m_i/m_e = 200$. The tearing is stabilized by an increase of β until $\beta = 0.4\%$, where the frequency changes from the electron ($\omega_r < 0$) to the ion ($\omega_r > 0$) diamagnetic drift direction (a). On the $q = 2$ surface, the dominant poloidal mode of the $n = 1$ amplitude of A_{\parallel} is $m = 3$ for $\omega_r > 0$, as shown in the left panel of (b).

aspect ratio A augments it. The frequency moderately increases and reduces with m_i/m_e and A . The mode $m/n = 3/1$ is thus behaving in an opposite manner to the $m/n = 2/1$ tearing mode which becomes more and more stable with increasing pressure gradient, β , mass ratio m_i/m_e and aspect ratio A .

C. Propagation of Nonlinear Islands

As mentioned in Sec. (I), the island rotation frequency is an important quantity for the determination of the stability of magnetic islands at the beginning of their nonlinear phase, as it influences both the polarization and the bootstrap current. The polarization current is proportional to $(\omega - \omega_e^*)(\omega - \omega_i^*)$ if the island size is below the typical ion-orbit size and the ion response can be assumed to be adiabatic (unmagnetized), while it is proportional to $\omega(\omega - \omega_i^*)$ in the large-island limit (flattened profiles).⁴⁶ For the bootstrap current, when the island size is comparable with the ion orbit size, the adiabatic ion response implies that the bootstrap current perturbation is strong when the island rotates in the ion diamagnetic di-

rection and weak when it rotates in the electron direction.⁴² For a collisionless drift tearing mode, the rotation frequency ω of a magnetic island is given by

$$\omega \cong \langle \omega^* \rangle + \langle \tilde{\omega}_{E \times B} \rangle \quad (18)$$

where $\langle \dots \rangle$ is a radial average over the island width and $\omega^* = \omega_{lin}^* + \tilde{\omega}^*$ the diamagnetic frequency,⁴⁸ ω_{lin} is the contribution from the gradients before the nonlinear interaction of the island with the surrounding plasma. The zonal flows and the pressure profile flattening play important roles in the island evolution. In particular, there is a relation between the flattening of the pressure profile within the island and the nonlinear generation of zonal flows, proportional to the Reynolds and Maxwell stresses, but also to the nonlinear ion diamagnetic stress related to the pressure profile gradient.^{50,86,87} The latter becomes important in the zonal flow generation mechanism for large islands as pressure profiles are strongly flattened.⁵⁰ Furthermore, the electrostatic potential has the role of providing an $E \times B$ flow that ensures $E_{\parallel} = 0$ within the island.⁵⁵ In the case of a magnetic island with imposed rotation velocity, the total electron frequency within the island is $\omega_{tot,e} = \omega_{pe}^* + \omega_{E \times B}$ which simplifies to $\omega_{tot,e} \cong \omega_{E \times B}$ when the pressure profile is flattened.⁴³

The nonlinear evolution of the tearing mode is investigated for finite temperature gradients using $-R_0 \nabla T_i / T_i = -R_0 \nabla T_e / T_e \equiv -R_0 / L_T = 2$ and 4 (for the density we take $-R_0 \nabla n / n = 0$), for $\beta = 0.07\%$ and 0.012%. The gradients are selected such that ITG, TEM or KBM modes are kept under their linear stability threshold.^{82,88–90} Fig. 20 shows the time evolution of the tearing mode amplitude and its real frequency ω_{TM} . The growth rate and saturation size decrease with increasing β and/or temperature gradients, as expected from the results presented above. The increased stability of the mode implies that the strong island decay observed for $\beta < 0.07\%$ with flat density and temperature profile is slightly seen for $-R_0 \nabla T / T = 2$ and $\beta = 0.07\%$ only. The rotation frequency reduces (in absolute value) when the island approaches saturation, then it changes to the ion diamagnetic direction. This behavior has been observed before in two-fluid simulations.^{5,49}

In order to investigate the change of rotation frequency, we scrutinize the pressure profile and zonal flows as the island appears and grows in size. We perform nonlinear simulations with $n \in [0, 30]$ in order to compare the island size $W \propto \sqrt{|A_{\parallel,21}|}$, its rotation frequency, the time evolution of the zonal flows and ω_* averaged over the island width or close to the rational surface.

First, we investigate profile flattening which is linked to the diamagnetic frequencies (first term in Eq. (18)) for the case $\beta = 0.07\%$ with $-R_0 \nabla T / T = 2$ (red curves in Fig. 20). The temperature profiles and their gradients for both species are depicted in Fig. 21. At the end of the simulation, the electron temperature profile clearly flattens over the island while the ions show a weak response. It should be stressed that the pressure profile flattening within the island is underestimated in the plots, because the flux surface average considered in the temperature computation includes contributions from the X-points. The weak response of the ion temperature profile

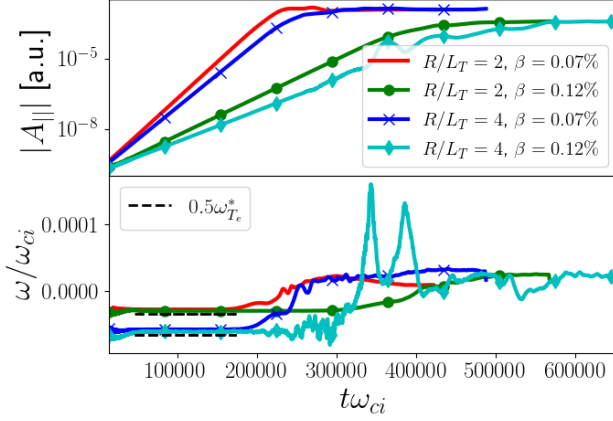


Figure 20 – $|A_{||,21}|$ and its real frequency ω_r time evolution for $\beta = 0.07\%$, 0.12% , $-R_0\nabla T/T = 2$ and 4 . The plasma β and $-R_0\nabla T/T$ decrease the growth rate. The mode frequency transitions from the electron to the ion drift diamagnetic direction between the linear and nonlinear evolution. The black dashed lines represents the linear electron diamagnetic drift $0.5\omega_{T_e}^*$.

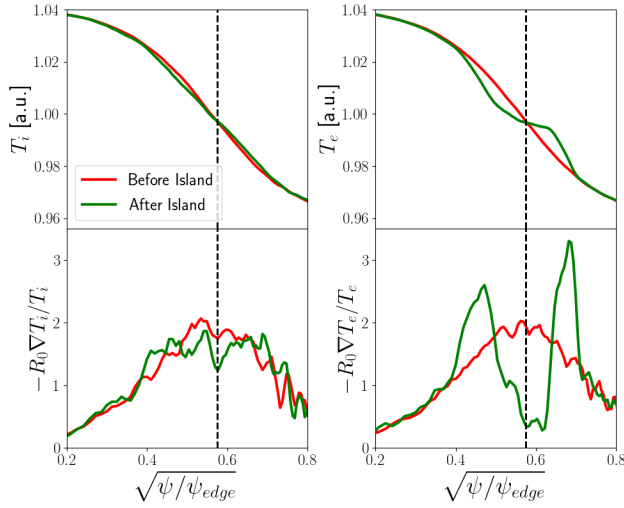


Figure 21 – Radial profiles of the ion and electron temperature and gradients before and after the island appearance. The electrons strongly flattens while the ions weakly respond to islands. A flux surface average is used to compute the temperature profiles.

is furthermore related to the ion banana width at the resonant surface $q = 2$

$$w_b = q_s \rho_i \sqrt{2A_s}, \quad (19)$$

with $A_s = R_0/r_s$ and q_s the aspect ratio and safety factor at the resonant surface. Using $q_s = 2$ and $r_s = 0.57$, Eq. (19) gives $w_b \cong 10\rho_i$ while the full island width $W \cong 20\rho_i$.

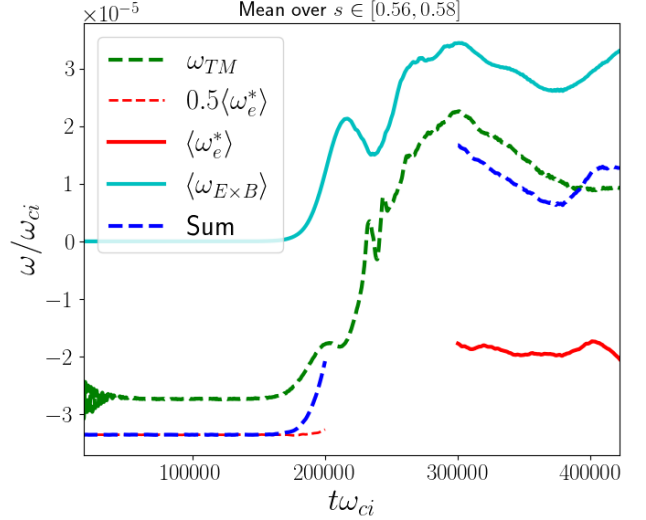


Figure 22 – Time trace of the tearing mode (ω_{TM}) in green, electron diamagnetic (ω_e^*) frequencies in red, zonal flows ($\omega_{E\times B}$) in cyan and the sum $\omega_e^* + \omega_{E\times B}$ in blue for $\beta = 0.07\%$ and $-R_0\nabla T/T = 2$. A flux surface average is applied on the zonal flow and the temperatures used to compute diamagnetic frequencies. Linearly ω_{TM} is close to $0.5\langle\omega_{T_e}^*\rangle$ while nonlinearly ω_{TM} approaches $\langle\omega_{E\times B}\rangle + \langle\omega_{T_e}^*\rangle$.

The overlap between the trapped ions and the magnetic island is significant, the ion response to the island is weak as the temperature profile flattening.⁴³ In particular, only few ions can be trapped within the island and their contribution to the pressure profile flattening is weak while the trapped ions were shown to be responsible for the density profile flattening in gyrokinetic simulations, using slab geometry together with a model to include toroidal effects, of imposed magnetic islands for which $w_{b_i} \ll W$.⁹¹ Fig. 22 shows the time evolution of the zonal flow (cyan curve), tearing mode (green dashed curve), electron diamagnetic frequency (red curve) and the sum of zonal flow with the electron drifts (dark blue dashed-curve). A flux surface average is considered to compute the zonal flows as well as the temperatures of the species that are used to compute the diamagnetic frequencies. These quantities are further radially averaged around the rational surface while the island frequency is computed at the rational surface. In the exponential growth (“linear”) phase, the contribution of the $E \times B$ velocity to the island rotation is negligible, and the rotation frequency is close to $0.5\omega_{T_e}^*$, as expected from theory and found also in previous gyrokinetic simulations.^{52,72,75} As the tearing mode leaves the linear phase and approaches saturation, its frequency turns to the ion diamagnetic direction, following the evolution of zonal flows time variation. The final island velocity is comparable to the sum of the zonal flow and the electron diamagnetic frequency (dark blue dashed-curve). The island frequency obtained here is different than previous gyrokinetic simulations, in slab geometry, that found an almost zero frequency of the island for gradients below the

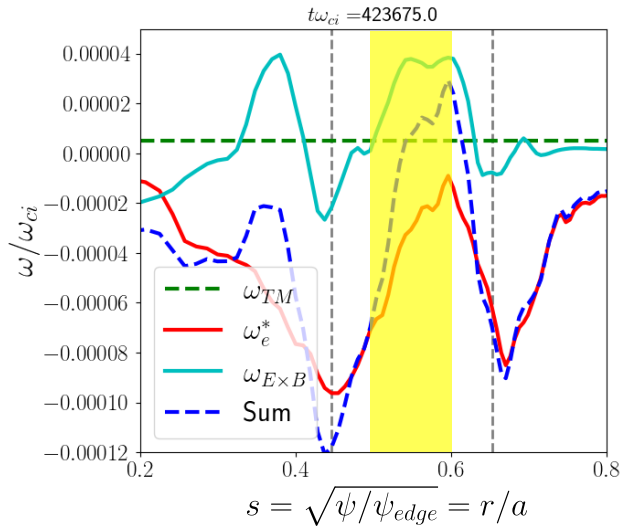


Figure 23 – Tearing mode (ω_{TM} in green), electron diamagnetic (ω_e^* in red) and zonal flows ($\omega_{E \times B}$ in cyan) frequencies radial profiles at the end of the simulations $\beta = 0.07\%$ and $-R_0 \nabla T/T = 2$. The resonant surface $q = 2$ is at $s = \sqrt{\psi/\psi_{edge}} = 0.57$ and vertical gray dashed-lines represent the island separatrix. The blue-dashed line is the sum of the zonal flow and the electron diamagnetic drift $\omega_{E \times B} + \omega_e^*$.

linear threshold of micro-instability.⁷⁵ The absence of collisions in our simulations explains this difference as there is no damping of the poloidal rotation without neoclassical viscous force.⁹² In such a case, the poloidal velocity of the island is mostly related to ϕ . Fig. 23 shows the flux surface average radial profiles of the $\mathbf{E} \times \mathbf{B}$ shear flow, tearing and electron diamagnetic drift frequencies at the simulation end. The potential that develops starting from $t\omega_{ci} \cong 2 \cdot 10^5$ is consistent with the frozen-in condition for the electrons, i.e., the sum (dark blue curve) of electron diamagnetic velocity (red curve) and $\mathbf{E} \times \mathbf{B}$ velocity (cyan curve) matches closely the island speed (green dashed curve) when averaged in the vicinity of the rational surface $s \in [0.5, 0.6]$ (yellow shaded box). This had been verified in previous gyrokinetic results,⁴³ where, however, the rotation of the island was imposed in the simulations and not self-consistently determined.

V. SUMMARY

In this paper, we presented a numerical gyrokinetic study of the tearing mode in a large-aspect-ratio tokamak. The mode develops because of a tearing-unstable current profile, initialized through a shifted Maxwellian as equilibrium distribution function for the electrons. The equilibrium is prescribed in such a way that the safety-factor profile is consistent with the corresponding equilibrium parallel electron flow. The simulations were performed in the collisionless

limit, so that the electron inertia is responsible for the breaking of the frozen-in condition $E_{\parallel} = 0$ around the rational surface. To reduce the computational burden and allow wide parameter scans, the mass ratio was fixed to $m_i/m_e = 200$ in most of the simulations. The initial temperature and density gradients were kept below the threshold for turbulent instabilities to develop, so that we could focus on the linear and nonlinear dynamics of the tearing instability. There are two aspects of the dynamics of magnetic island caused by tearing modes. One is its width, the other is the rotation. The former is investigated performing mainly simulations for flat profiles, because the rotation frequency is very small compared to the island growth in the absence of background diamagnetic flow effects, and the later is addressed carrying out simulations for finite gradient profiles as diamagnetic effects are responsible for the large rotation speed of the mode, at least in its linear phase.

We showed that, in the linear phase, the tearing mode follows the theoretical scaling for the growth rate and found that it exhibits a weak rotation frequency even without pressure gradients. For our parameters, the sign of this residual frequency, related to curvature effects, depends on β , being negative (what would be the electron diamagnetic direction in the presence of gradients) for $\beta \leq 0.07\%$ and positive otherwise. Nonlinear simulations demonstrate that, for strongly driven modes (which in our setup are realized through $\beta \leq 0.07\%$ and $m_i/m_e = 200$), the magnetic island width is dramatically reduced shortly after the initial saturation of its growth. The mechanism is composed of two subsequent processes:

1. Current redistribution: a strongly driven tearing mode produces large magnetic islands that generate nonlinearly significant zonal fields $A_{\parallel}(m = 0, n = 0)$. The related redistribution of the current profile lead to a reduced island drive and an initial shrinking of the island.
2. Island-induced flows: strongly driven tearing modes generate intense $\mathbf{E} \times \mathbf{B}$ and diamagnetic flows, with helicity $m/n = 2/1$, at the island separatrix because of localized electrostatic potential and quadrupolar density distribution around the X-points. These fields eventually become unstable to Kelvin-Helmholtz instability which then modifies the flow patterns. Strong outflows from the X-points, particularly intense in the presence of trapped electrons, lead to a violent shrinking of the island size.

While the current redistribution process, which initiates the island decrease, independent of the generation of the electrostatic turbulence, the latter is crucial for the further island decay, as it enhances the island generated flows responsible for its saturation. It is remarked that retaining a sufficient number of toroidal modes in the simulation turns out to be essential for capturing the current redistribution as well as the turbulence generation in their full extent. These strongly-driven scenarios are of interest for strongly driven magnetic islands like in sawtooth reconnection.⁹³ Obviously, the parameters considered in our simulations cannot be considered realistic and the electron mass, in particular, is artificially in-

creased for numerical convenience. This, however, can be regarded as a way to achieve a strong drive of the mode, which in realistic situations may be enforced through other physical processes.

Including density and temperature gradients, whose values are selected to avoid the destabilization of micro-instabilities, linear simulations reveal that the tearing mode growth rate is reduced by diamagnetic effects increasing $-R_0 \nabla T_i / T_i$ and $-R_0 \nabla n / n$ at low plasma β value. For $\nabla T_i / T_i \gg \nabla T_e / T_e$ the tearing rotates in the ion diamagnetic direction, while it rotates in the electron direction if the ion and electron pressure gradients are comparable, or larger for the electrons. At large plasma β and pressure gradients, the tearing mode is suppressed and is replaced by a mode with twisting parity coupled to a mode with helicity $m/n = 3/1$, whose growth rate and frequency increase with β and the pressure gradient. Its frequency is close to $0.5\omega_{Ti}^*$ when $-R_0 \nabla n / n = 0$. Additional work is required to determine the nature of this mode which bears similarities with KBM or AITG modes. The reduction of the linear growth rate in the presence of finite pressure gradients results also in a smaller island width at saturation. An island decay, as observed for flat profiles, is found in weaker form only for $-R_0 \nabla T / T = 2$, $\beta = 0.05\%$ and mass ratio $m_i / m_e = 200$, i.e., for parameters close to those used in flat-profile simulations. Concerning the mode rotation, nonlinear simulations with equal electron and ion temperature gradients were performed. The tearing mode is found to rotate in the electron diamagnetic drift direction, regardless of the plasma β value. When the island grows, the rotation frequency (in the electron direction in the linear phase) is reduced in absolute value as the electron pressure profile flattens within the island. The ion temperature profile weakly changes in response to the island because there is a significant overlap of the ion banana and island width $W/w_b \cong 2$. At saturation, the island rotates in the ion diamagnetic drift direction and this change of rotation direction is associated to the nonlinear production of zonal flows. We verified that the $\mathbf{E} \times \mathbf{B}$ flows generated by the island are consistent with the fulfillment of the frozen-in condition. This reversal of the rotation direction during its evolution plays a role in its neoclassical dynamics and will be further investigated in the near future in the presence of micro-turbulence. On a longer run, inclusion of collisions in the numerical setup will lead to an exploration of the neoclassical processes that affect the dynamics of the tearing mode and allow a comparison with theory, see e.g.⁹⁴ and references therein.

VI. ACKNOWLEDGMENTS

This work was carried out (partially) using supercomputer resources, JFRS-1 provided under the EU-JA Broader Approach collaboration in the Computational Simulation Centre of International Fusion Energy Research Centre (IFERC-CSC). Furthermore, part of this work has been carried out within the framework of the EUROfusion Consortium, funded by the European Union via the Euratom Research and Training Programme (Grant Agreement No.

101052200—EUROfusion). Views and opinions expressed are however those of the authors only and do not necessarily reflect those of the European Union or the European Commission. Neither the European Union nor the European Commission can be held responsible for them. This work was supported in part by the Swiss National Science Foundation. Simulations presented in this work were performed partially on the MARCONI FUSION HPC system at CINECA. We acknowledge PRACE for awarding us access to Marconi100 at CINECA, Italy. We acknowledge PRACE for awarding us access to Joliot-Curie at GENCI@CEA, France. One of the author (FW) would like to thank M. Muraglia, O. Agullo for fruitful discussions during the first European Conference on Magnetic Reconnection in Plasma in May 2023, Marseille, France. FW would also like to thank A. Poyé from the Aix-Marseille University for providing is shooting algorithm and his help using it. Additionally, we are grateful to M.J. Pueschel and T. Jitsuk for the code comparison with the GENE code and enlightening discussions. This research was carried out during the time the author (FW) was employed by the National Institutes of Natural Sciences (NINS). EP would like to thank the Graduate School of Energy Science of the Kyoto University for its hospitality and support during the finalization of this study. EP is partially supported by the Eurofusion Enabling Research Project (CfP-FSD-AWP24-ENR T-RecS). Finally, AM, AB and THS were partially supported by Eurofusion Theory and Simulation Verification and Validation Task 10.

REFERENCES

- ¹H. P. Furth, P. H. Rutherford, and H. Selberg, “Tearing mode in the cylindrical tokamak,” *Physics of Fluids* **16**, 1054–1063 (1973).
- ²M. Yamada, R. Kulsrud, and H. Ji, “Magnetic reconnection,” *Reviews of Modern Physics* **82**, 603–664 (2010).
- ³D. Biskamp, *Magnetic Reconnection in Plasmas*, Vol. 3 (2000).
- ⁴O. Sauter, R. J. La Haye, Z. Chang, D. A. Gates, Y. Kamada, H. Zohm, A. Bondeson, D. Boucher, J. D. Callen, M. S. Chu, T. A. Gianakon, O. Gruber, R. W. Harvey, C. C. Hegna, L. L. Lao, D. A. Monticello, F. Perkins, A. Pletzer, A. H. Reiman, M. Rosenbluth, E. J. Strait, T. S. Taylor, A. D. Turnbull, F. Waelbroeck, J. C. Wesley, H. R. Wilson, and R. Yoshino, “Beta limits in long-pulse tokamak discharges,” *Physics of Plasmas* **4**, 1654–1664 (1997).
- ⁵A. Ishizawa, Y. Kishimoto, and Y. Nakamura, “Multi-scale interactions between turbulence and magnetic islands and parity mixture—a review,” *Plasma Physics and Controlled Fusion* **61**, 054006 (2019).
- ⁶“Resistive mhd stability,” in *Magnetohydrodynamic Stability of Tokamaks* (John Wiley & Sons, Ltd, 2014) Chap. 8, pp. 123–140, <https://onlinelibrary.wiley.com/doi/pdf/10.1002/9783527677375.ch8>.
- ⁷R. Carrera, R. D. Hazeltine, and M. Kotschenreuther, “Island bootstrap current modification of the nonlinear dynamics of the tearing mode,” *Physics of Fluids* **29**, 899–902 (1986).
- ⁸M. Kotschenreuther, R. D. Hazeltine, and P. J. Morrison, “Nonlinear dynamics of magnetic islands with curvature and pressure,” *Physics of Fluids* **28**, 294–302 (1985).
- ⁹B. Carreras, H. R. Hicks, and D. K. Lee, “Effects of toroidal coupling on the stability of tearing modes,” *Physics of Fluids* **24**, 66–77 (1981).
- ¹⁰F. Widmer, P. Maget, O. Février, H. Lütjens, and X. Garbet, “Non-linear simulations of neoclassical tearing mode control by externally driven RF current and heating, with application to ITER,” *Nuclear Fusion* **59**, 106012 (2019).
- ¹¹H. Reimerdes, O. Sauter, T. Goodman, and A. Pochelon, “From Current-Driven to Neoclassically Driven Tearing Modes,” *Phys. Rev. Lett.* **88**,

- 105005 (2002).
- ¹²E. Poli, A. Bergmann, F. J. Casson, W. A. Hornsby, A. G. Peeters, M. Siccinio, and D. Zarzoso, "Kinetic effects on the currents determining the stability of a magnetic island in tokamaks," *Plasma Physics Reports* **42**, 450–464 (2016).
 - ¹³E. Poli, A. Bottino, and A. G. Peeters, "Behaviour of turbulent transport in the vicinity of a magnetic island," *Nuclear Fusion* **49**, 075010 (2009).
 - ¹⁴E. Poli, A. Bottino, W. A. Hornsby, A. G. Peeters, T. Ribeiro, B. D. Scott, and M. Siccinio, "Gyrokinetic and gyrofluid investigation of magnetic islands in tokamaks," *Plasma Physics and Controlled Fusion* **52**, 124021 (2010).
 - ¹⁵W. A. Hornsby, A. G. Peeters, E. Poli, M. Siccinio, A. P. Snodin, F. J. Casson, Y. Camenen, and G. Szepesi, "On the nonlinear coupling between micro turbulence and mesoscale magnetic islands in a plasma," *EPL (Europhysics Letters)* **91**, 45001 (2010).
 - ¹⁶W. A. Hornsby, A. G. Peeters, A. P. Snodin, F. J. Casson, Y. Camenen, G. Szepesi, M. Siccinio, and E. Poli, "The nonlinear coupling between gyroradius scale turbulence and mesoscale magnetic islands in fusion plasmas," *Physics of Plasmas* **17**, 092301 (2010).
 - ¹⁷R. E. Waltz and F. L. Waelbroeck, "Gyrokinetic simulations with external resonant magnetic perturbations: Island torque and nonambipolar transport with plasma rotation," *Physics of Plasmas* **19**, 032508 (2012).
 - ¹⁸D. Zarzoso, F. J. Casson, W. A. Hornsby, E. Poli, and A. G. Peeters, "Verification of a magnetic island in gyro-kinetics by comparison with analytic theory," *Physics of Plasmas* **22**, 022127 (2015).
 - ¹⁹A. Bañón Navarro, L. Bardóczi, T. A. Carter, F. Jenko, and T. L. Rhodes, "Effect of magnetic islands on profiles, flows, turbulence and transport in nonlinear gyrokinetic simulations," *Plasma Physics and Controlled Fusion* **59**, 034004 (2017).
 - ²⁰J.-M. Kwon, S. Ku, M. J. Choi, C. S. Chang, R. Hager, E. S. Yoon, H. H. Lee, and H. S. Kim, "Gyrokinetic simulation study of magnetic island effects on neoclassical physics and micro-instabilities in a realistic KSTAR plasma," *Physics of Plasmas* **25**, 052506 (2018).
 - ²¹K. S. Fang and Z. Lin, "Global gyrokinetic simulation of microturbulence with kinetic electrons in the presence of magnetic island in tokamak," *Physics of Plasmas* **26**, 052510 (2019).
 - ²²M. Muto, K. Imadera, and Y. Kishimoto, "Effects of magnetic island on profile formation in flux-driven ITG turbulence," *Physics of Plasmas* **29**, 052503 (2022).
 - ²³J. Li, J. Q. Xu, Y. R. Qu, Z. Lin, J. Q. Dong, X. D. Peng, and J. Q. Li, "Global gyrokinetic simulations of the impact of magnetic island on ion temperature gradient driven turbulence," *Nuclear Fusion* **63**, 096005 (2023), arXiv:2306.05607 [physics.plasm-ph].
 - ²⁴W. A. Hornsby, P. Migliano, R. Buchholz, D. Zarzoso, F. J. Casson, E. Poli, and A. G. Peeters, "On seed island generation and the non-linear self-consistent interaction of the tearing mode With electromagnetic gyrokinetic turbulence," *Plasma Physics and Controlled Fusion* **57**, 054018 (2015), arXiv:1409.0648 [physics.plasm-ph].
 - ²⁵W. A. Hornsby, P. Migliano, R. Buchholz, S. Grosshauser, A. Weikl, D. Zarzoso, F. J. Casson, E. Poli, and A. G. Peeters, "The non-linear evolution of the tearing mode in electromagnetic turbulence using gyrokinetic simulations," *Plasma Physics and Controlled Fusion* **58**, 014028 (2016), arXiv:1507.02841 [physics.plasm-ph].
 - ²⁶D. Zarzoso, S. Nasr, X. Garbet, A. I. Smolyakov, and S. Benkadda, "Gyro-kinetic theory and global simulations of the collisionless tearing instability: The impact of trapped particles through the magnetic field curvature," *Physics of Plasmas* **26**, 112112 (2019).
 - ²⁷T. Jitsuk, A. Di Siena, M. J. Pueschel, P. W. Terry, F. Widmer, E. Poli, and J. S. Sarff, "Global linear and nonlinear gyrokinetic simulations of tearing modes," *Nuclear Fusion* **64**, 046005 (2024), arXiv:2308.16345 [physics.plasm-ph].
 - ²⁸W. Wan, Y. Chen, and S. E. Parker, "Gyrokinetic δf simulation of the collisionless and semicollisional tearing mode instability," *Physics of Plasmas* **12**, 012311 (2005).
 - ²⁹B. N. Rogers, S. Kobayashi, P. Ricci, W. Dorland, J. Drake, and T. Tatsuno, "Gyrokinetic simulations of collisionless magnetic reconnection," *Physics of Plasmas* **14** (2007), 10.1063/1.2774003.
 - ³⁰M. J. Pueschel, F. Jenko, D. Told, and J. Büchner, "Gyrokinetic simulations of magnetic reconnection," *Physics of Plasmas* **18**, 112102 (2011).
 - ³¹O. Zacharias, R. Kleiber, and R. Hatzky, "Gyrokinetic simulations of collisionless tearing modes," in *Journal of Physics Conference Series*, Journal of Physics Conference Series, Vol. 401 (2012) p. 012026.
 - ³²Y. Yao, Z. Lin, J. Q. Dong, P. Shi, S. F. Liu, and J. Li, "Gyrokinetic simulations of double tearing modes in toroidal plasma," *Physics Letters A* **417**, 127681 (2021).
 - ³³A. Mishchenko, A. Bottino, T. Hayward-Schneider, E. Poli, X. Wang, R. Kleiber, M. Borchardt, C. Nührenberg, A. Biancalani, A. Könies, E. Lanti, P. Lauber, R. Hatzky, F. Vannini, L. Villard, and F. Widmer, "Gyrokinetic particle-in-cell simulations of electromagnetic turbulence in the presence of fast particles and global modes," *Plasma Physics and Controlled Fusion* **64**, 104009 (2022), arXiv:2203.11983 [physics.plasm-ph].
 - ³⁴S. Jolliet, A. Bottino, P. Angelino, R. Hatzky, T. Tran, B. Mcmillan, O. Sauter, K. Appert, Y. Idomura, and L. Villard, "A global collisionless PIC code in magnetic coordinates," *Computer Physics Communications* **177**, 409–425 (2007).
 - ³⁵E. Lanti, B. F. McMillan, S. Brunner, N. Ohana, and L. Villard, "Gradient- and flux-driven global gyrokinetic simulations of ITG and TEM turbulence with an improved hybrid kinetic electron model," *Journal of Physics: Conference Series* **1125**, 012014 (2018).
 - ³⁶H. R. Wilson, J. W. Connor, R. J. Hastie, and C. C. Hegna, "Threshold for neoclassical magnetic islands in a low collision frequency tokamak," *Physics of Plasmas* **3**, 248–265 (1996).
 - ³⁷S. Günter, G. Gantenbein, A. Gude, V. Igochine, M. Maraschek, A. Mück, S. Saarelma, O. Sauter, A. C. C. Sips, H. Zohm, and ASDEX Upgrade Team, "Neoclassical tearing modes on ASDEX Upgrade: improved scaling laws, high confinement at high β_N and new stabilization experiments," *Nuclear Fusion* **43**, 161–167 (2003).
 - ³⁸R. J. Buttery, T. C. Hender, D. F. Howell, R. J. L. Haye, O. Sauter, D. Testa, and contributors to the EFDA-JET Workprogramme, "Onset of neoclassical tearing modes on {JET}," *Nuclear Fusion* **43**, 69 (2003).
 - ³⁹E. Poli, A. Bergmann, A. G. Peeters, L. C. Appel, and S. D. Pinches, "Kinetic calculation of the polarization current in the presence of a neoclassical tearing mode," *Nuclear Fusion* **45**, 384–390 (2005).
 - ⁴⁰F. L. Waelbroeck, F. Militello, R. Fitzpatrick, and W. Horton, "Effect of electrostatic turbulence on magnetic islands," *Plasma Physics and Controlled Fusion* **51**, 15015 (2009).
 - ⁴¹A. Ishizawa and F. L. Waelbroeck, "Magnetic island evolution in the presence of ion-temperature gradient-driven turbulence," *Physics of Plasmas* **20**, 122301 (2013).
 - ⁴²A. Bergmann, E. Poli, and A. G. Peeters, "The bootstrap current in small rotating magnetic islands," *Physics of Plasmas* **16**, 092507 (2009).
 - ⁴³M. Siccinio, E. Poli, F. J. Casson, W. A. Hornsby, and A. G. Peeters, "Gyrokinetic determination of the electrostatic potential of rotating magnetic islands in tokamaks," *Physics of Plasmas* **18**, 122506 (2011).
 - ⁴⁴B. Coppi, "Influence of Gyration Radius and Collisions on Hydromagnetic Stability," *Physics of Fluids* **7**, 1501–1516 (1964).
 - ⁴⁵D. Biskamp, "Drift-tearing modes in a tokamak plasma," *Nuclear Fusion* **18**, 1059–1068 (1978).
 - ⁴⁶A. I. Smolyakov, H. Search, C. Journals, A. Contact, M. Iopscience, P. Phys, and I. P. Address, "Nonlinear evolution of tearing modes in inhomogeneous plasmas," *Plasma Physics and Controlled Fusion* **35**, 657 (1993).
 - ⁴⁷F. L. Waelbroeck, "Theory and observations of magnetic islands," *Nuclear Fusion* **49**, 104025 (2009).
 - ⁴⁸S. Nishimura, S. Benkadda, M. Yagi, S. I. Itoh, and K. Itoh, "Nonlinear dynamics of rotating drift-tearing modes in tokamak plasmas," *Physics of Plasmas* **15**, 1–10 (2008).
 - ⁴⁹M. Muraglia, O. Agullo, M. Yagi, S. Benkadda, P. Beyer, X. Garbet, S.-I. Itoh, K. Itoh, and A. Sen, "Effect of the curvature and the β parameter on the nonlinear dynamics of a drift tearing magnetic island," *Nuclear Fusion* **49**, 055016 (2009).
 - ⁵⁰K. Uzawa, A. Ishizawa, and N. Nakajima, "Propagation of magnetic island due to self-induced zonal flow," *Physics of Plasmas* **17**, 42508 (2010).
 - ⁵¹A. Ishizawa, F. L. Waelbroeck, R. Fitzpatrick, W. Horton, and N. Nakajima, "Magnetic island evolution in hot ion plasmas," *Physics of Plasmas* **19** (2012), 10.1063/1.4739291.
 - ⁵²J. F. Drake and Y. C. Lee, "Kinetic theory of tearing instabilities," *Physics of Fluids* **20**, 1341–1353 (1977).
 - ⁵³J. F. Drake, "Stabilization of the tearing mode in high-temperature plasma," *Physics of Fluids* **26**, 2509 (1983).

- ⁵⁴S. Nishimura, M. Yagi, S.-I. Itoh, M. Azumi, and K. Itoh, “Thermal Transport Effects on Drift-Tearing Mode,” *Journal of the Physical Society of Japan* **76**, 064501 (2007).
- ⁵⁵A. I. Smolyakov, A. Hirose, E. Lazzaro, G. B. Re, and J. D. Callen, “Rotating nonlinear magnetic islands in a tokamak plasma,” *Physics of Plasmas* **2**, 1581–1598 (1995).
- ⁵⁶M. Sato and A. Ishizawa, “Nonlinear parity mixtures controlling the propagation of interchange modes,” *Physics of Plasmas* **24**, 082501 (2017).
- ⁵⁷E. Lanti, N. Ohana, N. Tronko, T. Hayward-Schneider, A. Bottino, B. F. McMillan, A. Mishchenko, A. Scheinberg, A. Biancalani, P. Angelino, S. Brunner, J. Dominski, P. Donnel, C. Gheller, R. Hatzky, A. Jocksch, S. Jolliet, Z. X. Lu, J. P. Martin Collar, I. Novikau, E. Sonnendrücker, T. Vernay, and L. Villard, “ORB5: A global electromagnetic gyrokinetic code using the PIC approach in toroidal geometry,” *Computer Physics Communications* **251**, 107072 (2020), arXiv:1905.01906 [physics.plasm-ph].
- ⁵⁸A. Mishchenko, A. Bottino, A. Biancalani, R. Hatzky, T. Hayward-Schneider, N. Ohana, E. Lanti, S. Brunner, L. Villard, M. Borchart, R. Kleiber, and A. Könies, “Pullback scheme implementation in ORB5,” *Computer Physics Communications* **238**, 194–202 (2019), arXiv:1811.05346.
- ⁵⁹Y. Chen and S. Parker, “Gyrokinetic turbulence simulations with kinetic electrons,” *Physics of Plasmas* **8**, 2095–2100 (2001).
- ⁶⁰A. Mishchenko, R. Hatzky, and A. Könies, “Conventional δf -particle simulations of electromagnetic perturbations with finite elements,” *Physics of Plasmas* **11**, 5480–5486 (2004).
- ⁶¹A. Bottino, T. Vernay, B. Scott, S. Brunner, R. Hatzky, S. Jolliet, B. F. McMillan, T. M. Tran, and L. Villard, “Global simulations of tokamak microturbulence: finite- β effects and collisions,” *Plasma Physics and Controlled Fusion* **53**, 124027 (2011).
- ⁶²A. Mishchenko, M. Cole, R. Kleiber, and A. Könies, “New variables for gyrokinetic electromagnetic simulations,” *Physics of Plasmas* **21**, 052113 (2014).
- ⁶³A. Mishchenko, A. Könies, R. Kleiber, and M. Cole, “Pullback transformation in gyrokinetic electromagnetic simulations,” *Physics of Plasmas* **21**, 092110 (2014), arXiv:1407.3992 [physics.plasm-ph].
- ⁶⁴J. Wesson and D. Campbell, *Tokamaks 4th Edition*, International Series of Monographs on Physics (OUP Oxford, 2011).
- ⁶⁵The number is found to be sufficient by a convergence test.
- ⁶⁶R. G. Kleva, J. F. Drake, and F. L. Waelbroeck, “Fast reconnection in high temperature plasmas,” *Physics of Plasmas* **2**, 23–34 (1995).
- ⁶⁷N. Jain, J. Büchner, and P. A. Muñoz, “Nonlinear evolution of electron shear flow instabilities in the presence of an external guide magnetic field,” *Physics of Plasmas* **24**, 032303 (2017), arXiv:1608.02403 [physics.plasm-ph].
- ⁶⁸M. J. Pueschel, P. W. Terry, D. Told, and F. Jenko, “Enhanced magnetic reconnection in the presence of pressure gradients,” *Physics of Plasmas* **22** (2015), 10.1063/1.4922064.
- ⁶⁹A. Ishizawa and N. Nakajima, “Thermal transport due to turbulence including magnetic fluctuation in externally heated plasma,” *Nuclear Fusion* **49** (2009), 10.1088/0029-5515/49/5/055015.
- ⁷⁰N. Arcis, D. F. Escande, and M. Ottaviani, “Nonlinear dynamics of the tearing mode for any current gradient [rapid communication],” *Physics Letters A* **347**, 241–247 (2005).
- ⁷¹N. Arcis, D. F. Escande, and M. Ottaviani, “Rigorous approach to the nonlinear saturation of the tearing mode in cylindrical and slab geometry,” *Physics of Plasmas* **13**, 052305 (2006), arXiv:physics/0603204 [physics.plasm-ph].
- ⁷²W. A. Hornsby, P. Migliano, R. Buchholz, L. Kroenert, A. Weigl, A. G. Peeters, D. Zarzoso, E. Poli, and F. J. Casson, “The linear tearing instability in three dimensional, toroidal gyro-kinetic simulations,” *Physics of Plasmas* **22**, 022118 (2015), arXiv:1408.0112 [physics.plasm-ph].
- ⁷³F. Jenko, W. Dorland, M. Kotschenreuther, and B. N. Rogers, “Electron temperature gradient driven turbulence,” *Physics of Plasmas* **7**, 1904–1910 (2000).
- ⁷⁴Although the equilibrium pressure is flat in these simulations, we refer to the diamagnetic direction as the direction in which a given particle species would rotate in the presence of a finite gradient.
- ⁷⁵W. A. Hornsby, P. Migliano, R. Buchholz, S. Grosshauser, A. Weigl, D. Zarzoso, F. J. Casson, E. Poli, and A. G. Peeters, “The non-linear evolution of the tearing mode in electromagnetic turbulence using gyrokinetic simulations,” *Plasma Physics and Controlled Fusion* **58**, 014028 (2016).
- ⁷⁶D. Grasso, D. Borgogno, E. Tassi, and A. Perona, “Asymmetry effects driving secondary instabilities in two-dimensional collisionless magnetic reconnection,” *Physics of Plasmas* **27**, 012302 (2020).
- ⁷⁷D. Borgogno, D. Grasso, B. Achilli, M. Romé, and L. Comisso, “Coexistence of Plasmoid and Kelvin-Helmholtz Instabilities in Collisionless Plasma Turbulence,” *apj* **929**, 62 (2022).
- ⁷⁸C. Granier, E. Tassi, D. Laveder, T. Passot, and P. L. Sulem, “Influence of ion-to-electron temperature ratio on tearing instability and resulting subion-scale turbulence in a low- β_e collisionless plasma,” *Physics of Plasmas* **31**, 032115 (2024), arXiv:2311.01539 [physics.plasm-ph].
- ⁷⁹R. L. Fermo, J. F. Drake, and M. Swisdak, “Secondary Magnetic Islands Generated by the Kelvin-Helmholtz Instability in a Reconnecting Current Sheet,” *pri* **108**, 255005 (2012).
- ⁸⁰F. Porcelli, “Collisionless $m=1$ tearing mode,” *pri* **66**, 425–428 (1991).
- ⁸¹E. Tassi, F. L. Waelbroeck, and D. Grasso, “Gyrofluid simulations of collisionless reconnection in the presence of diamagnetic effects,” in *Journal of Physics Conference Series*, Journal of Physics Conference Series, Vol. 260 (2010) p. 012020, arXiv:1109.0092 [physics.plasm-ph].
- ⁸²S. Maeyama, A. Ishizawa, T. H. Watanabe, M. Nakata, N. Miyato, M. Yagi, and Y. Idomura, “Comparison between kinetic-ballooning-mode-driven turbulence and ion-temperature-gradient-driven turbulence,” *Physics of Plasmas* **21** (2014), 10.1063/1.4873379.
- ⁸³A. Ishizawa, S. Maeyama, T. H. Watanabe, H. Sugama, and N. Nakajima, “Electromagnetic gyrokinetic simulation of turbulence in torus plasmas,” *Journal of Plasma Physics* **81** (2015), 10.1017/S0022377815000100.
- ⁸⁴F. Zonca, L. Chen, J. Q. Dong, and R. A. Santoro, “Existence of ion temperature gradient driven shear Alfvén instabilities in tokamaks,” *Physics of Plasmas* **6**, 1917–1924 (1999).
- ⁸⁵G. L. Falchetto, J. Vaclavik, and L. Villard, “Global-gyrokinetic study of finite β effects on linear microinstabilities,” *Physics of Plasmas* **10**, 1424–1436 (2003).
- ⁸⁶F. L. Waelbroeck, “Natural Velocity of Magnetic Islands,” *Physical Review Letters* **95**, 35002 (2005).
- ⁸⁷R. J. L. Haye, C. C. Petty, E. J. Strait, F. L. Waelbroeck, and H. R. Wilson, “Propagation of magnetic islands in the $E_r = 0$ frame of co-injected neutral beam driven discharges in the DIII-D tokamak,” *Physics of Plasmas* **10**, 3644–3648 (2003).
- ⁸⁸W. Horton, “Drift waves and transport,” *Reviews of Modern Physics* **71**, 735–778 (1999).
- ⁸⁹F. Rytter, C. Angioni, A. G. Peeters, F. Leuterer, H.-U. Fahrbach, and W. Suttrop (ASDEX Upgrade Team), “Experimental study of trapped-electron-mode properties in tokamaks: Threshold and stabilization by collisions,” *Phys. Rev. Lett.* **95**, 085001 (2005).
- ⁹⁰T. Dannert and F. Jenko, “Gyrokinetic simulation of collisionless trapped-electron mode turbulence,” *Physics of Plasmas* **12**, 072309 (2005).
- ⁹¹D. Zarzoso, W. A. Hornsby, E. Poli, F. J. Casson, A. G. Peeters, and S. Nasr, “Impact of rotating magnetic islands on density profile flattening and turbulent transport,” *Nuclear Fusion* **55**, 113018 (2015).
- ⁹²A. I. Smolyakov, A. Hirose, E. Lazzaro, G. B. Re, and J. D. Callen, “Rotating nonlinear magnetic islands in a tokamak plasma,” *Physics of Plasmas* **2**, 1581–1598 (1995).
- ⁹³D. Biskamp and T. Sato, “Partial reconnection in the nonlinear internal kink mode,” *Physics of Plasmas* **4**, 1326–1329 (1997).
- ⁹⁴A. V. Dudkova, J. W. Connor, D. Dickinson, P. Hill, I. K., S. Leigh, and H. R. Wilson, “Drift kinetic theory of neoclassical tearing modes in a low collisionality tokamak plasma: magnetic island threshold physics,” *Plasma Physics and Controlled Fusion* **63**, 054001 (2021).